2023

Photocatalytic reforming of lignocellulose: A review

Xinyuan Xu
Edith Cowan University

Lei Shi

Shu Zhang

Zhimin Ao

Jinqiang Zhang

See next page for additional authors

10.1016/j.cej.2023.143972
Xu, X., Shi, L., Zhang, S., Ao, Z., Zhang, J., Wang, S., & Sun, H. (2023). Photocatalytic reforming of lignocellulose: A review. *Chemical Engineering Journal, 469,* article 143972. https://doi.org/10.1016/j.cej.2023.143972

Chemical Engineering Journal 469 (2023) 143972

Contents lists available at ScienceDirect

Chemical Engineering Journal

journal homepage: www.elsevier.com/locate/cej

Review

Photocatalytic reforming of lignocellulose: A review

Xinyuan Xu [a], Lei Shi [b], Shu Zhang [b], Zhimin Ao [c], Jinqiang Zhang [d], Shaobin Wang [d], Hongqi Sun [a,*]

[a] School of Science, Edith Cowan University, 270 Joondalup Drive, Joondalup, WA 6027, Australia
[b] Joint International Research Laboratory of Biomass Energy and Materials, Co-Innovation Center of Efficient Processing and Utilization of Forest Resources, College of Materials Science and Engineering, Nanjing Forestry University, Nanjing 210037, Jiangsu, China
[c] Advanced Interdisciplinary Institute of Environment and Ecology, Beijing Normal University, Zhuhai 519087, China
[d] School of Chemical Engineering, The University of Adelaide, Adelaide, SA 5005, Australia

ARTICLE INFO

Keywords:
Photocatalysis
Reforming
Semiconductor
Lignocellulose
C-O linkages

ABSTRACT

Biomass has been considered as a promising energy resource to combat the exhaustion of fossil fuels, as it is renewable, sustainable, and clean. Photocatalytic reforming is a novel technology to utilize solar energy for upgrading biomass in relatively mild conditions. This process efficiently reforms and recasts biomass into hydrogen and/or valuable chemicals. To date, lignocellulose, including cellulose, hemicellulose and lignin, has attracted extensive studies in facile photocatalytic valorisation. This review summarizes and analyzes the most recent research advances on photoreforming of lignocellulose to provide insights for future research, with a particular emphasis on the reformation of lignin because of its 3D complex and stubborn structure. The structure of lignin contains a dominant linkage, i.e., β-O-4. The breakage of β-O-4 linkage can be proceeded by two steps, e.g., oxidization and reduction, according to the sequence of photoexcited holes and electrons. Thus, this review discusses two-step and integrate step dissociation strategies along with the rationally chosen photocatalysts. The challenges of the photocatalysts, solvent, and post-treatment were identified, and potential solutions to these challenges were provided.

1. Introduction

The excessive consumption of fossil fuels is a pressing issue that poses a challenge to sustainable energy supply and environmental protection. Carbon emissions and air pollution, which are the result from the consumption and combustion of fossil fuels, are global concerns [1]. Therefore, hydrogen has been urged to replace fossil fuels because it has inherent merits of being clean, sustainable, and renewable to environment [2–4]. However, the current methods for hydrogen production, such as electrolysis and reforming using fossil fuels, consume significant amounts of energy and involve steam to produce hydrogen at high pressures and temperatures (15-40 bar and 650-950 °C) [5,6]. Furthermore, the generated hydrogen needs further purification to remove impurities [7]. Since Fujishima and Honda's discovery of photocatalytic water splitting to release hydrogen via a TiO_2 electrode in 1972, there has been worldwide interest in this approach [8].

Despite decades of research, photocatalytic hydrogen evolution remains a low efficiency because of the high recombination of photoexcited electrons and holes that occurs in the bulk of semiconductors, leading to a low apparent quantum efficiency [9]. In 1980, Kawai and Sakata innovatively introduced a sacrificial agent derived from biomass, i.e., methanol, into the process of photocatalytic hydrogen generation. Methanol was oxidized by the photoinduced holes to suppress the recombination rate, and then to greatly promote the efficiency in hydrogen generation [10]. In the same year, they also reported a photocatalytic process of biomass on a ternary composite, $RuO_2/TiO_2/Pt$ to produce CO_2 and H_2 [11]. Since then, more organic components with simple structures, such as ethanol, glycerol and ethylene glycol, have been utilized as efficient sacrificial agents in the photocatalytic process. These organic sacrificial agents can be easily derived from renewable raw biomass to improve hydrogen generation, as shown in the stoichiometric yield equation below [12].

$$C_xH_yO_z + (2x - z)H_2O \xrightarrow{h\nu} xCO_2 + \left(2x - z + \frac{y}{2}\right)H_2 \quad (1)$$

After that, the photocatalytic process has been extensively studied for not only the hydrogen generation process but also the oxidization of

* Corresponding author.
E-mail address: h.sun@ecu.edu.au (H. Sun).

https://doi.org/10.1016/j.cej.2023.143972
Received 16 March 2023; Received in revised form 22 May 2023; Accepted 5 June 2023
Available online 10 June 2023

organic sacrificial agents. Studies have shown that biomass-derived sacrificial agents, such as organic polymeric components with complex and complicated structures, can be oxidized and reduced by photogenerated electron-hole pairs to produce more value-added chemicals [13]. This demonstrates that photocatalysts can facilitate the oxidative and reductive chemistry from their excited states during the photocatalytic depolymerization [14–16], leading to the emergence of a new attractive field called photoreforming [17–19]. Photoreforming involves the depolymerization of biomass into valuable hydrogen and chemicals using solar energy at ambient pressure and temperature, thereby avoiding the thermal energy input required in traditional reforming technologies [20–23].

Lignocellulose, a renewable carbon feedstock source, has been investigated over the years for providing valuable chemicals and fuels [24–27]. It is produced on an annual basis with the most complicated structure on the earth by photosynthesis [28–30]. This kind of biomass can be supplied by the food residues of crops and non-agricultural lands. Theoretically, 50-85 EJ/year energy, around 20% energy demand of the society, can be provided by these residues, with roughly 3-5 Gt/year productivity all over the world [31]. Lignocellulose has been utilized mainly by two approaches, e.g., biological and chemocatalytic processes [32,33]. While fermentation and enzymatic catalysis can break the lignocellulose with the support of enzymes, bacteria and microorganisms during a biological process [34,35], this method is of a low efficiency due to the intricate structure of lignocellulose that hinders the contact between the enzymes and biomass [36].

Chemocatalytic technology can be categorized into three main processes, e.g., gasification, pyrolysis and hydrolysis [31,37]. Traditional gasification is the most common chemocatalytic process to decompose the complex structure of lignocellulose at high temperatures above 750 °C, releasing hydrogen, carbon oxide, carbon dioxide and methane [37,38]. However, the high temperature and pressure make the process demanding, and harsh reaction conditions introduce undesired degradation products, leading to unsatisfactory selectivity of final products [39,40].

In contrast, photocatalytic conversion of lignocellulose, especially lignin, in ambient conditions was recently proposed as an alternative method to the traditional process, bridging the two renewable energies of solar energy and biomass together (Fig. 1) [41–44]. Many publications over the past few decades have investigated the photocatalytic lignocellulose reforming. Typically, Reisner's group proposed the photoreforming of real solid waste streams for a carbon-neutral objective [23], while Sun's group collected and discussed photoreforming performances over a variety of modified carbon nitride [45]. Moreover, Amal's team focused on improving the selectivity of photocatalysts for water abatement [46]. However, the intricate mechanisms of photocatalytic reforming on the basis of lignocellulose over different photocatalysts have not been well collected and evaluated [29]. This review comprehensively analyzes and evaluates the photocatalytic reforming of some substances in lignocellulose, namely glucose, cellulose, hemicellulose (monomers) and lignin, on the basis of performances of hydrogen evolution and biomass depolymerization. Additionally, it also emphasizes the photocatalytic selective depolymerization of lignin by the dissociation of C-C and C-O bonds. Therefore, this review can provide a variety of innovative and creative ideas to underpin future development in this field.

2. Photocatalytic reforming fundamentals

2.1. Thermodynamics of biomass reforming

Photocatalytic reforming of biomass under ambient pressure and temperature relies heavily on the use of semiconductors which can produce hot electrons and holes after being activated by photons with a higher energy than the semiconductor's bandgap energy [46]. Specifically, electrons can be excited and separated from valence band (VB), then immigrated to conduction band (CB), leaving hot holes in VB. The excited electrons in CB reduce H_2O to generate hydrogen, while holes drive the biomass oxidation process in VB as displayed in the Fig. 1 (right-hand side). There is a challenge in accurately controlling partial oxidation to prevent complete mineralization of the biomass into CO_2 [47]. Thus, identifying the energy range that simultaneously activates semiconductors and produces biomass-derived intermediates and understanding the thermodynamic fundamentals of hydrogen generation and biomass reforming is essential for successful photoreforming.

The thermodynamic barrier of hydrogen evolution in water splitting is -1.23 V vs. RHE [48]. Nonetheless, the biomass photocatalytic conversion reaction has a nearly energy-neutral barrier of 0.001 V vs. RHE, making it feasible under not only UV light but almost the entire solar spectrum [29]. This low thermodynamic barrier allows photoreforming to occur under mild conditions. The photogenerated charge carriers play an indispensable role in photocatalytic biomass reforming. The

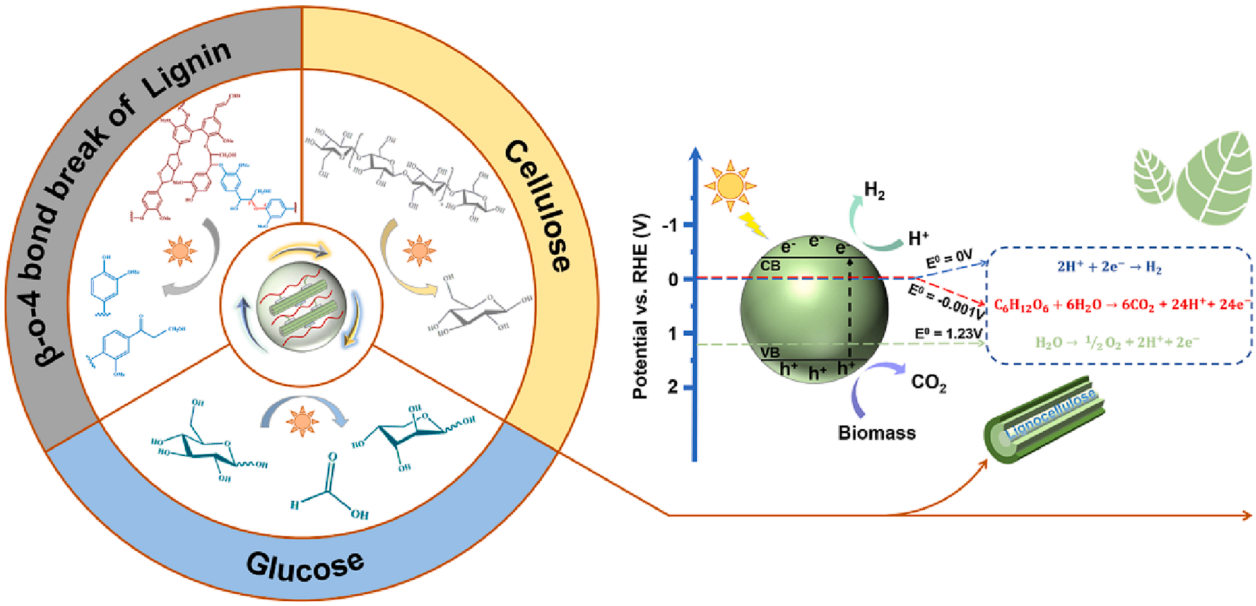

Fig. 1. Photocatalytic reforming of lignocellulose into value-added chemicals via semiconductor-based photocatalysis.

photoinduced electrons and holes can react with both hydroxyl groups and dissolved oxygen to generate reactive oxygen species (ROS). The photoinduced holes can immediately oxidize the biomass to generate biomass-based radicals that sustain the process of biomass reforming [49,50]. It is known that photoreforming process follows two different pathways, depending on the generation of different radicals, with or without oxygen. Firstly, the photogenerated holes and electrons can directly oxidize and reduce dissolved hydroxyl and oxygen to form hydroxyl (·OH) with a redox potential of 2.81 V vs SHE (standard hydrogen electrode) and superoxide radicals ($\cdot O_2^-$) with a redox potential of -0.89 V vs SHE [51]. It is noted that superoxide radicals can only be generated under aerobic conditions, where oxygen is necessary to react with electrons. Although superoxide radicals can enhance the degree of chemoselectivity, some negative effects can emerge, producing undesired products instead of the target final products [52]. Therefore, controlling and optimizing the generation of valuable chemicals and hydrogen is important in the photocatalytic reforming reaction.

2.2. Structural potentials of lignocellulose in photocatalytic reforming

Lignocellulose is the most abundant biomass all over the world and the annual production of it is around 200 billion metric tons [28]. It consists of three basic biopolymers: cellulose, hemicellulose and lignin, along with a limited number of other substances such as minerals, phenolic substituents and acetyl groups [53]. These polymers are combined and interacted to form cross-linked organic structures that provide resistance against corrosion, degradation and UV damage from ambient environment [54,55].

As exhibited in the Fig. 2, cellulose, the most abundant substance in lignocellulose, constitutes approximately 40 wt% and has a generic formula of $(C_6H_{12}O_5)_n$ [57–59]. It is made up of glucose units that are connected by bonding networks of intermolecular and intramolecular force to maintain stability as the scaffold and prohibit the hydrolysis process [57]. Additionally, Hemicellulose covers cellulose and consists of pentose and hexose sugars, accounting for around 20-40 wt% [20]. There are five sugar monomers in hemicellulose, including D-galactose, D-xylose, D-mannose, D-glucose and L-arabinose [60]. Meanwhile, lignin is a 35 wt% 3D amorphous phenolic polymer component that encapsulates hemicellulose and cellulose in lignocellulose. The lignin content can vary depending on the botanical species, with 30% of total mass isolated from softwood lignin, 20-25% from hardwood, and 10-15% from grass lignin [61,62]. To be more specific, it is the richest aromatic polymers source in the world and consists of three different primary phenylpropanoid units, e.g., coniferyl alcohol (4-hydroxy-3-methoxy-cinnamyl), sinapyl alcohol (3,5-dimethoxy-4-hydroxycinnamyl) and p-coumaryl alcohol (4-hydroxycinnamyl) [63–66]. As such, softwood and hardwood lignin can be harvested by the different distribution of these alcoholic moieties. Softwood lignin is composed by around 90% coniferyl alcohols, which is equivalent to the sum of sinapyl and coniferyl alcohols in hardwood [67]. These units are highly irregularly cross-jointed and interlinked by C-C and C-O.

Notably, β-O-4 is the most common bond of the C-O linkages in the lignin structure, accounting for 43-70% of the structure and this exclusive linkage can be more likely broken [68–70]. The abundance of β-O-4 is able to be increased to around 89% through bioengineering to promote the highest efficiency in the reformation of lignin [71]. However, the complicated and stubborn structure of lignin impedes the hydrolysis and fermentation to destroy the matrix of plants, making it a challenge in photocatalytic depolymerization to produce phenolic substances and other alcohols [43,72,73]. As a result, a large amount of lignin substances is used in industries such as paper and pulp as a source of power by combustion because of its high calorific value [74]. The unique structure of lignocellulose with abundant valuable chemicals offers great potentials in photocatalytic reforming processes, which will then be discussed in detail. Herein, a few typical model compounds with their exclusive linkages, e.g., glucose, cellobiose (β-1,4-glycosidic bonds), xylose, xylan and 2-phenoxy-1-phenylethanol (β-O-4), were chosen to replace the lignocellulose into the photocatalytic reforming process as simple models before practical lignocellulose reforming. The comprehensive mechanism can be clearly explained after the bond dissociation by photoreforming, and then the outcomes can highly promote the efficiency in the utilization of lignocellulose.

2.3. Pre-treatment strategies of biomass

Chemical and physical properties of the substrates are also important in photoreforming [75,76]. Biomass pre-treatment methods can be generally categorized into chemical, physical, biological approaches and combination strategies [77]. As such, chemical pre-treatment methods mainly include alkaline, acid and ionic liquids pre-treatment, while microwave, ultrasound and mechanical pre-treatment are usually involved in physical pre-treatment strategy. Meanwhile, the use of microorganisms and enzymes can be ascribed to biological pre-treatment. Notably, both of chemical and physical pre-treatment can achieve a higher efficiency than biological pre-treatment [78]. Furthermore, photocatalysis can also exhibit the possible enhancement in biomass pre-treatment by generating active radicals to proceed the selective conversion of lignocellulose. It is noteworthy that the higher hydrogen evolution and biomass conversion can be monitored on the basis of pre-treated biomass compared with untreated raw biomass [79]. Thus, the investigations of biomass pre-treatment should be carefully considered and widely explored to promote the efficiency in the photoreforming reactions.

3. Photocatalytic reforming of glucose as the basic unit of cellulose

Sugars have been widely employed and investigated in photocatalytic conversion because the saccharide monomers are the basic units of lignocellulose. Moreover, cellulose is also composed of the repeated connection of D-glucose units [80]. As the representative unit of lignocellulosic biomass substances, glucose has been strategically studied to acquire insights into photocatalytic reforming (sugar aldose).

In 1980, Kawai and Sakata reported on the photocatalytic hydrogen

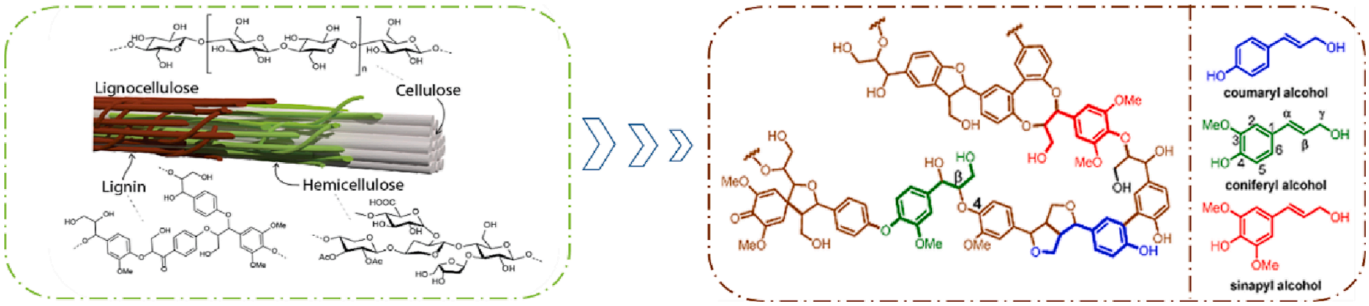

Fig. 2. Structures of lignocellulose (cellulose, hemicellulose and lignin) [20,56].

generation through the reforming of sugar, starch, and cellulose over $RuO_2/TiO_2/Pt$ [11]. Since then, TiO_2 has been widely utilized as a common semiconductor because of its stability, high efficiency and non-toxicity [81]. However, TiO_2 owns the large bandgap (3.2 eV) which impedes the utilization of visible light, resulting in low efficiency in the use of solar energy [81]. Hence, TiO_2 needs to be modified to boost the utilization of overall solar energy and the efficiency of reforming.

One effective method of modifying TiO_2 is through depositing the noble metal cocatalysts on itself, such as Pt, Au, Rh, and Pd. Fu et al. reported the performance of 1.0 wt% noble metals loaded on pure anatase TiO_2 via the impregnation and reduction process. Results showed that 1.0 wt% Pt loaded TiO_2 exhibited the highest performance, greatly improving the rate of hydrogen generation to around 4.08 mmol $g_{cat}^{-1}h^{-1}$ in the initial 5 h reaction in a 1.39×10^{-3} mol L^{-1} glucose solution (Table 1) [82]. The highest hydrogen evolution rate was achieved when 50 mg of glucose was dissolved in an aqueous solution (200 mL), and a higher concentration could not further increase the H_2 evolution amount due to the saturation between the surface of the photocatalyst and glucose molecule based on Langmuir-Hinshelwood [83].

In addition, a mechanism was reported by Fu et al. to explain the mechanism in Fig. 3. The hydroxyl group of molecule glucose attaches with Ti atoms and dissociates to H^+ and $RCH_2\text{-}O^-$ in the process (a). Meanwhile, $RCH_2\text{-}O^-$ was oxidized to produce $RCH_2O^{\cdot}$ radicals by trapping photoexcited holes. These radicals simultaneously reacted with other glucose molecules by transferring the radical electrons to the C atoms of the glucose molecules. Those glucose molecules will be reduced to form R'CHOH radicals that can be deprotonated to form R'CHO by repeating the process (a) (process (b)). Moreover, the oxidization of R'CHO can introduce $[R'COOH]^-$ to the process due to the surface bound hydroxyl radicals. Besides, R'H and CO_2 can be generated and emitted by the photo-kolbe reaction based on decarboxylation in the process (c) [84]. Finally, hydrogen will be generated by the reduction of H^+ provided by the deprotonated glucose.

Furthermore, Au, Pd, Ag and Rh were also investigated and loaded on the surface of mixed crystal TiO_2 (P-25-mixture structure of rutile 25% and anatase 75%), which can offer higher activity than anatase phase. Gomathisankar et al. reported that the highest hydrogen generation occurred on Au and Pd modified TiO_2 (P25) with a photodecomposition method. These modified TiO_2 significantly enhanced the efficiency of hydrogen generation in aqueous glucose solutions, with the hydrogen generation performance of Au and Pd modified TiO_2 increasing to around 203 and 362 times, respectively, that of pure TiO_2 [85]. Besides, Wu et al. introduced Rh into the photocatalytic reforming system and achieved a hydrogen release rate of 1.45 mmol $g_{cat}^{-1}h^{-1}$ in a 5 h reaction under irradiations [86].

Non-noble metals have been considered as alternatives to noble metals as cocatalysts because of their lower costs and ability to enhance the optical properties of TiO_2. Cu loaded TiO_2 was synthesized and showed a comparable performance (1.07 mmol $g_{cat}^{-1}h^{-1}$ in 5 h) to Rh/TiO_2 in the photocatalytic reforming process [86]. In addition, CO was also detected in the glucose reforming process as a by-product, which could be ascribed to the reformation of formic acid species resulting from the oxidation of glucose molecules and the dissociation of C-C bond. According to the theory proposed by John et al., aldehyde and hydroxyl functional groups of glucose can be oxidized on Pt/TiO_2 by photocatalysis, generating protons and carboxyls [87]. Thus, these results can undoubtedly prove that glucose molecule was successfully reformed. Meanwhile, Ni/TiO_2 (P25) was prepared for glucose reforming process, which released hydrogen at a rate of approximately 0.08 mmol $g_{cat}^{-1}h^{-1}$ in 5.5 h [88]. Heteroatom-doped TiO_2, such as B and N-doped TiO_2 (platinized), synthesized by Luo et al., achieved a hydrogen evolution rate of 2.19 mmol $g_{cat}^{-1}h^{-1}$ in the glucose reforming process [89].

To enhance visible light absorption and achieve better utilization of light, metallic oxides, chalcogenides, and carbon-based materials have also been investigated. Cuprous oxide, a metallic oxide catalyst (p-type) with a 2.0 eV bandgap, has an approximately 18% conversion efficiency in an ideal light-to-hydrogen program by AM 1.5 spectrum [90]. As such, multifaceted Cu_2O was introduced by Zhang et al. into the glucose reforming system, achieving a hydrogen generation rate of 0.019 mmol $g_{cat}^{-1}h^{-1}$ in 6 h [90]. Two iron oxide polymorphs, $\beta\text{-}Fe_2O_3$ and $\varepsilon\text{-}Fe_2O_3$, were synthesized and employed in the glucose reforming reaction to overcome the photocatalytic limits of $\alpha\text{-}Fe_2O_3$ [91]. According to the report from Carraro et al., the rate of hydrogen evolution (5.7 mmol $m^{-2}h^{-1}$) was achieved after 9 h reaction on $\beta\text{-}Fe_2O_3$. Meanwhile, another phase of iron oxide, $\varepsilon\text{-}Fe_2O_3$, can reach 9.2 mmol $m^{-2}h^{-1}$ in 11 h reaction.

The deposition of ZnS on the ternary sulfide $ZnIn_2S_4$ was evidenced

Table 1
Photocatalytic hydrogen evolution in the reforming process of glucose.

Photocatalyst	Solvent	Concentration of Glucose	Light Source	Atmosphere	Illumination Time (h)	Hydrogen Generation (mmol $g_{cat}^{-1}h^{-1}$/ mmol $m^{-2}h^{-1}$)	Ref.
1.0 wt% Pt/TiO_2 (50 mg)	DI-Water (30 °C)	1.39×10^{-3} mol L^{-1}	High-pressure mercury lamp (125 W)	N_2 (>99.99%)	5	4.08	[82]
Au/TiO_2 (20 mg)	Aqueous solution (50 °C)	1.00 mol L^{-1}	LED lamp (365 nm)	-	1	5.00	[85]
Pd/TiO_2 (20 mg)	Aqueous solution (50 °C)	1.00 mol L^{-1}	LED lamp (365 nm)	-	1	8.90	[85]
0.3% Rh/TiO_2 (500 mg)	Aqueous solution	1.25×10^{-3} mol L^{-1}	High-pressure Hg lamp (300 W)	Vacuum	5	~1.45	[86]
0.3% Cu/TiO_2 (500 mg)	Aqueous solution	1.25×10^{-3} mol L^{-1}	High-pressure Hg lamp (300 W)	Vacuum	5	~1.07	[86]
0.2% Ni/TiO_2 (150 mg)	DI-Water (60 °C)	1.39×10^{-4} mol L^{-1}	Xe arc lamp (150 W)	Ar	5.5	~0.08	[88]
Pt-B, N/TiO_2 (50 mg)	Aqueous solution	2.76×10^{-1} mol L^{-1}	Xe lamp (300 W)	Ar	4	~2.19	[89]
Cu_2O (100 mg)	Aqueous and NaOH solution	1.25×10^{-2} mol L^{-1}	Xe lamp (300 W)	Ar	6	0.019	[90]
$\beta\text{-}Fe_2O_3$ (1 cm^2)	Aqueous solution (25 °C)	5.50×10^{-2} mol L^{-1}	Xe lamp (150 W)	-	9	~5.7	[91]
$\varepsilon\text{-}Fe_2O_3$ (1 cm^2)	Aqueous solution (25 °C)	5.50×10^{-2} mol L^{-1}	Xe lamp (150 W)	-	11	~9.2	[91]
ZnS-$ZnIn_2S_4$ (100 mg)	Aqueous solution	1.00×10^{-1} mol L^{-1}	Metal halide lamp (400 W)	N_2	10	0.103	[92]
ZMCN (50 mg)	Aqueous solution (30 °C)	5.52×10^{-5} mol L^{-1}	Xe lamp (300 W)	N_2	3	0.095	[93]
SNGODs (400 mg)	Aqueous solution (25 °C)	3.50×10^{-1} mol L^{-1}	Xe lamp (300 W)	-	12	~0.164	[94]

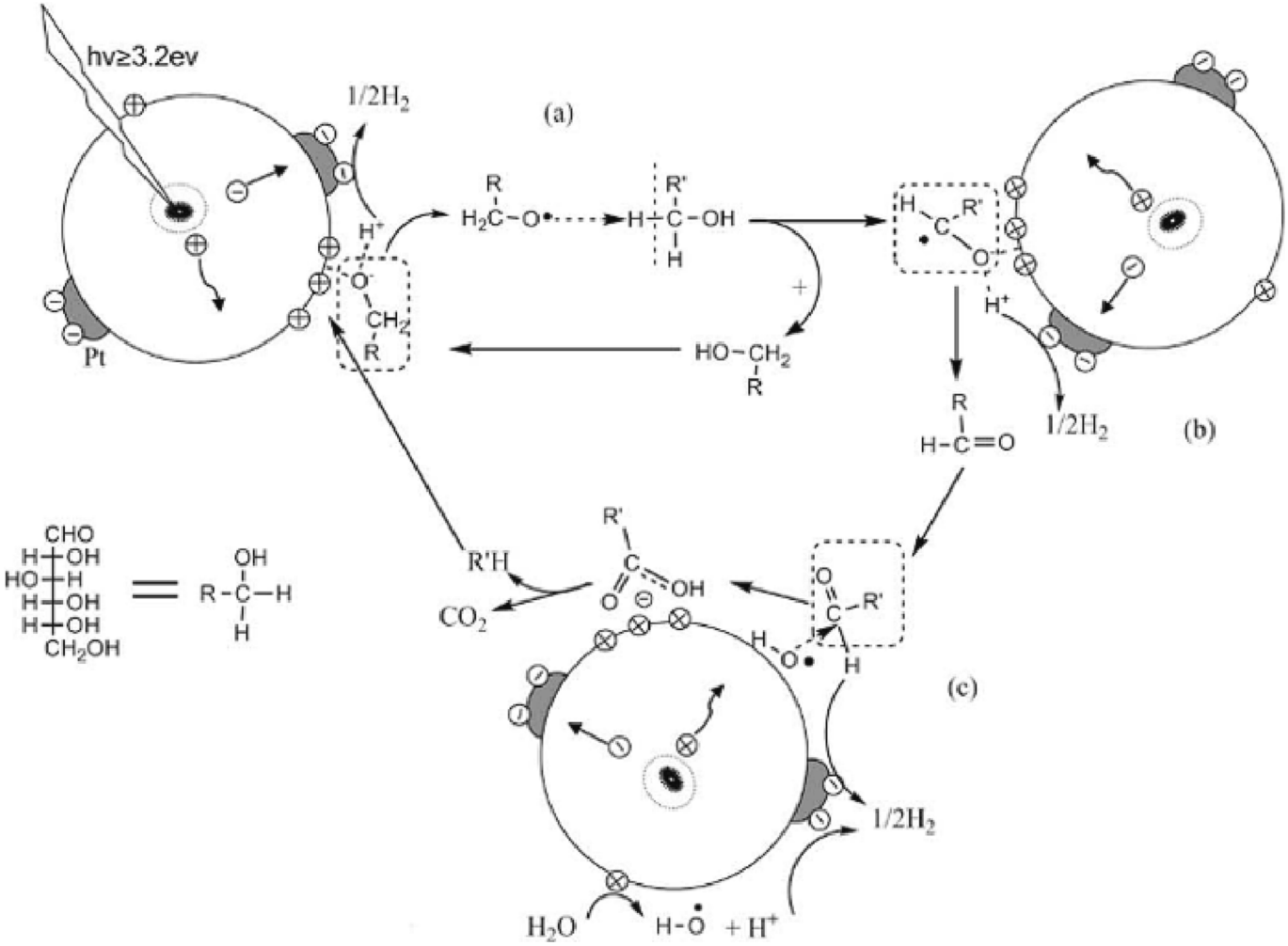

Fig. 3. Possible deduction of glucose reforming mechanism on the basis of Pt/TiO_2 [82].

that can rise the rate of hydrogen production up to 0.103 mmol $g_{cat}^{-1}h^{-1}$ in 10 h. As the first study on $ZnIn_2S_4$ in this process, it was found that ZnS can enhance the possibility of glucose molecule adsorbing on the surface of $ZnIn_2S_4$ [92]. Moreover, Xu et al. loaded ZnS nanoparticles on melamine synthesized g-C_3N_4 which can also improve the hydrogen production rate to around 0.095 mmol $g_{cat}^{-1}h^{-1}$ in 3 h [93]. It is worth mentioning that while sulfide catalysts can deliver high performances in biomass reforming system, chalcogenide catalysts are sensitive to be oxidized in this system. This is because S^{2-} can be self-oxidized by photoinduced holes to release electrons, supporting the reduction reaction of H^+ [92]. Based on these metal sulfides, it is significant to avoid the self-oxidized process by introducing the innovative modification methods.

Representative hydrogen generation results of glucose photoreforming process on various photocatalysts are provided in Table 1.

Carbon based photocatalyst materials have gained popularity as ideal catalysts due to their responsiveness to visible light and eco-friendliness [94]. In a recent study, S and N co-doped graphene oxide dots were applied into the photocatalytic system to promote the valorization of glucose, delivering a 0.164 mmol $g_{cat}^{-1}h^{-1}$ of hydrogen within a 12-h reaction. Additionally, the mechanism of glucose reforming process was systematically investigated by analyzing the liquid phase by-products after reaction. Colmenares et al. reported that the high value chemicals, for example, gluconic acid, arabitol and glucaric acid, can be gained via the selective reforming of glucose based on three TiO_2 related materials in 2011 [95].

Due to the less complicated structure of glucose compared to cellulose, glucose reformation studies have become more mature. Glucose can be easily reformed under mild conditions through irradiations onto a variety of photocatalysts, resulting in the production of hydrogen, CO, CO_2, glucaric acid, gluconic acid, and arabitol as by-products. Meanwhile, weak alkaline solution can favour the hydrogen generation based on the studies of 1.0 wt% Pt/TiO_2 (pH = 11) [82], Cu_2O (pH = 13) [90], ZnS-$ZnIn_2S_4$ (pH = 12.68) [92] and SNGODs (pH = 10) [94]. These studies provide strong support for the photoreforming of cellulose, with heteroatom-doped TiO_2, Pt-B, N/TiO_2, exhibiting better hydrogen production performances compared to other noble metal modified TiO_2. Boron doping can improve the utilization of visible light on TiO_2 by narrowing its bandgap, thereby offering innovative considerations for improving the visible light response of pristine TiO_2. As a result, these studies provide sufficient guidance for investigating the reforming of cellulose through more innovative photocatalysts at a larger scale.

4. Photocatalytic reforming of cellulose

Cellulose, the main non-edible substance of biomass, has attracted considerable attentions in the reforming field. It is worth noting that glucose units are interlinked by β-1,4-glycosidic in cellulose [96,97]. Breaking these bonds is crucial, but cellulose's recalcitrant structure makes it difficult to valorize and depolymerize under mild conditions, requiring high energy inputs in most reformation processes. Therefore, visible-light-driven photocatalytic reforming becomes more compelling.

Recent studies have explored novel photocatalysts for breaking

β-1,4-glycosidic bonds in cellulose. For example, Ir modified HY zeolite (Ir/HY) was demonstrated to cleave these bonds in cellobiose, a cellulose model compound composed of glucose dimers, when dissolved in EMIMCl solution and irradiated with visible light at 100 °C. The selectivity reached 99% due to the acid catalysis on HY zeolite and plasmonic photothermal effect over Ir. Meanwhile, a variety of HY zeolites with different proportions of Si/Al, for instance, HY (Si/Al = 7), HY_2 (Si/Al = 5.2) and HY_3 (Si/Al = 11), were employed in the hydrolysis of crystalline cellulose (non-pretreated). Ir/HY_3 showed an impressive yield of total products (75.3%), including 10.9% cellobiose, 40.4% glucose and 24.0% 5-HMF under visible light irradiations at 90 °C in Ar atmosphere [96].

TiO_2 nanofibre (NF) supported H-form Y-zeolites (HY) with the decoration of Au-NPs were successfully synthesized and proceeded into the photocatalytic hydrolysis of cellulose [98]. This elaborated photocatalyst (Au-HYT) achieved the yield of HMF and glucose of 10.6 and 48.1%, respectively, under the visible light irradiations at 140 °C. EMIMCl solution also played a key role in this photocatalytic hydrolysis reaction by assisting the hydrolysis of cellulose. Modified TiO_2 photocatalysts were also introduced for the cellulose reformation. The 0.5 wt % Pt/TiO_2 was synthesized through a facile photochemical deposition strategy [99]. The deposition of Pt led to a great enhancement of hydrogen generation compared to the pure TiO_2 because Pt can impede the recombination of photoexcited electron-hole as active sites. Simultaneously, the photo-excited holes, ·OH and O_2 from water cleavage can be captured by the cellulose to produce glucose and HMF products. Notably, this process was also successfully proceeded into the real cellulosic biomass reformation such as rice husk and alfalfa stems.

Another effective approach for promoting the hydrolysis of cellulose involves the one-pot decoration of TiO_2 with Ni_xS_y (Nickel Sulfide) and chemisorbed sulfate [100]. This approach significantly improved the hydrogen generation rate, reaching levels around 76 times higher than P25 within the first 3 h. The presence of Ni_xS_y acted as a cocatalyst, trapping electrons, while the introduced sulfate serves as a solid acid catalyst, facilitating the reformation of cellulose by oxidizing soluble glucose with photogenerated holes and releasing protons into the overall reaction. In another study by Zhang et al., TiO_2/NiO_x nanoparticles were loaded on a layer of graphitic carbon, which can efficiently promote the conversion of cellulose to the hydrogen production rate to around 4.15 mmol $g_{cat}^{-1}h^{-1}$ at 80 °C [101]. NiO_x nanoparticles were reduced by the photogenerated electrons under the irradiations, producing Ni on the surface of bulk TiO_2. The reduction of protons from alcohol adsorbed on the surface of Ni, in conjunction with electrons, yields an alkoxide anion and a Ni-H hydride. The interaction between Ni surface and H was weakened by the presence of carbon layer, thereby enhancing hydrogen evolution.

Immobilizing cellulose on the surface of TiO_2 enables its conversion into hydrogen and sugars upon irradiation without the need for a sacrificial agent. The immobilization of cellulose creates a ligand-to-metal-charge-transfer complex (LMCT), accelerating the transfer of electrons to the conduction band of the photocatalyst. The hybrid/cellulose system, obtained by mixing and drying cellulose with TiO_2, exhibited higher performance in cellulose conversion compared to TiO_2 alone. For instance, TC4, a TiO_2 sample with a cellulose fraction of 20.5 wt%, demonstrated efficient cellulose conversion by producing a variety of gas and liquid products within a 42-h reaction period [102].

Not only is the immobilization of cellulose a rather efficient approach, but the immobilized photocatalyst nanoparticles can also boost the cellulose reformation. CdS nanoparticles were immobilized on a porous cellulose (RC) film with diverse pore sizes [103]. The porous structure can efficiently confine the CdS nanoparticles in small sizes, improving the mobility of charge carrier to the surface of CdS. In this study, the highest hydrogen generation rate (1.344 mmol $g_{cat}^{-1}h^{-1}$) was observed over Pt-decorated CdS/RC-4.5 film, which had a cellulose concentration of 4.5 wt%, during 5 h of irradiation.

According to the collected studies above, it is possible to reform cellulose via a relative mild condition, e.g., low temperature and pressure, under light irritations. Ionic liquid, such as EMIMCl, efficiently enhances the photocatalytic reforming of cellulose by assisting in its hydrolysis. Therefore, further investigation of more efficient ionic liquids should be undertaken to expand the possibilities for cellulose hydrolysis. Additionally, the LMCT approach offers a new perspective to enhance the efficiency of cellulose reforming by immobilizing cellulose. Exploring the immobilization of biomass on the surface of other photocatalysts may also be attempted to optimize the reforming process.

5. Photocatalytic reforming of hemicellulose

Hemicellulose, a non-linear polysaccharide and amorphous, owns a lower degree of polymerization (50-200 monomers) compared to cellulose [104,105]. It is composed of a variety of monomers, including glucose, arabinose, xylose, mannose, galactose and glucuronic acid [106]. Specifically, the major sugars found in hemicellulose are xylans and mannans [107]. Meanwhile, the physical strength of hemicellulose is weak due to its short chains and less polymers aggregation. This unique structure makes the hemicellulose easier to be broke than cellulose. Thus, the potential for hydrogen production from xylose, the major sugar monomer from hemicellulose, should also be considered and studied in photoreforming.

Anatase TiO_2 was modified by biochar nanosheet, *a*-TiO_2@MC, to promote the mobility of charge carriers in the visible light driven photoreforming of xylose in the basic solution [108]. This modified photocatalyst achieved the yield of lactic acid (49.22%) in the alkali solution at a high temperature. Conversely, the yield of 52.26% xylonic acid was preferred to be collected at a low alkalinity and temperature under visible light illumination at 50 °C in 1 h. The performances demonstrated that h^+ played an essential role in the photoreforming reaction. Additionally, a 1000-fold scale-up experiment also proved that this elaborated photocatalyst could be employed for industrial production.

Another modified photocatalyst, $RuP_2/Ti_4P_6O_{23}$@TiO_2-7, was prepared using an evaporation-calcination approach [109]. The formation of active sites on the photocatalyst surface can decrease the recombination probability of photogenerated charge carriers. Besides, the introduction of RuP_2 and $Ti_4P_6O_{23}$ forms heterojunction, broadening the visible light utilization. Thus, the elaborated photocatalyst can synchronously provide 16.3 mmol $g_{cat}^{-1}h^{-1}$ and 87.87% yield of lactic acid from the photocatalytic reforming of arabinose in the alkali solution (5 M, 30 mL of KOH). Moreover, the hydrogen production of xylose (10.4 mmol $g_{cat}^{-1}h^{-1}$), mannose (3.7 mmol $g_{cat}^{-1}h^{-1}$), rhamnose (4.4 mmol $g_{cat}^{-1}h^{-1}$), fructose (8.1 mmol $g_{cat}^{-1}h^{-1}$) and glucose (5.9 mmol $g_{cat}^{-1}h^{-1}$) can also be collected via $RuP_2/Ti_4P_6O_{23}$@TiO_2-7 in the same reaction condition. The yield of xylose was 79.72%. This innovative modification can deliver a new concept in the field of photocatalytic reforming.

Additionally, a series of controllable C/N ratio photocatalysts, CC_1@mCN_x (x = 5, 10 and 15), were prepared and reported to harvest lactic acid from selective photocatalytic reforming of monosaccharides, such as xylose, mannose, glucose, fructose and arabinose [110]. Specifically, CC_1@mCN_{10} can exhibit the highest performance for converting xylose, rhamnose, mannose, arabinose, glucose and fructose into lactic acid, with yields of 76.82, 50.96, 64.13, 79.82, 69.90 and 57.46%, respectively. As such, active oxygen species (h^+, $\cdot O_2^-$, ·OH and $^1O_2$) were also investigated by adding isopropyl, ethylenediaminetetraacetic acid, tryptophan and benzoquinone into the reforming reaction. The results demonstrated that these active oxygen species are important in the production of lactic acid from xylose where $\cdot O_2^-$ is the major contributor. Notably, the success of 1000-fold scale-up experiments showed the potential for the industrial scale.

Oxygen-doped modified carbon nitride nanocages (O@CNNCs) also exhibited an excellent performance in the photocatalytic conversion of xylose and xylan. Meanwhile, xylonic acid can be obtained through the support of active oxygen species, including h^+, $\cdot O_2^-$, ·OH and $^1O_2$ [111]. The highest yield of xylonic acid (83.4%) was achieved by converting

xylose (95.9%) using 10 mL KOH (100 mmol/L), 20 mg of catalyst, and 100 mg of xylose at 70 °C for 1 h. When xylan was used instead of xylose under the same reaction conditions, a yield of xylonic acid of 0.77 g/gxylan was achieved. This novel photocatalyst presents a promising approach to improve the conversion of xylose and xylan.

In another study, BP-s-CN, a black phosphorus sensitized carbon nitride, was synthesized to enhance the hydrogen production and lactic acid yield from various monosaccharides, including xylose, mannose, arabinose, rhamnose, fructose, and glucose [112]. As such, the highest rate of hydrogen production (290 mmol $g_{cat}^{-1}h^{-1}$) was obtained through the photocatalytic oxidation of arabinose in a 6-h reaction using 5.0 mg of BP-s-CN, 150 mg of arabinose, 0.5 mL of 5.0 mM H_2PtCl_6, and 30 mL of 5.0 M KOH, with a lactic acid yield of 74.4%. Besides, the hydrogen evolutions for xylose, mannose, rhamnose, fructose and glucose were 264, 158, 266, 64 and 218 mmol $g_{cat}^{-1}h^{-1}$, with corresponding lactic acid yields of 64.4, 16.7, 9.9, 42.5 and 31.9%, respectively. The investigation of mechanism identified the significance of active oxygen species h^+, $\cdot O_2^-$, ·OH and $^1O_2$, while $\cdot O_2^-$ was a key factor in the photocatalytic oxidation process.

A single-atom modified carbon nitride, Zn-mCN, was synthesized via an innovative strategy (calcination-calcination-washing) and employed in the photoreforming of biomass-derived monosaccharides, including xylose, arabinose, mannose, rhamnose, glucose and fructose [113]. An excellent performance of hydrogen production (15.9 mmol $g_{cat}^{-1}h^{-1}$) was achieved through the synergistic effect of Zn-mCN, xylose and alkali solution in the photoreforming process. Meanwhile, the selectivity of lactic acid was up to 91.0%. Besides, the macromolecular xylan also exhibited a hydrogen production rate of 13.5 mmol $g_{cat}^{-1}h^{-1}$, with a lactic acid yield of 18.09 mg/300 mg. According to the mechanistic study, $\cdot O_2^-$ exhibited an indispensable role in the hydrogen evolution, while ·OH was related to the yield of lactic acid.

A range of 3D flexible self-supporting catalysts, e.g., CIS@FSM_{400}, CIS@FSM_{450}, CIS@FSM_{500}, were synthesized by varying their annealing temperature [114]. These materials were designed to optimize the photoreforming of xylose and maximize the yields of xylonic acid. The highest yield of xylonic acid (65.05%) was achieved by utilizing CIS@FSM450 (4 mg), 40 mg of xylose, 0.2 M KOH (4 mL), and a temperature of 60 °C over a 45-min reaction. Photogenerated h^+ was an important contributor in the selective conversion of xylose, demonstrating the efficiency of these materials in mild reaction environments.

Although photoreforming of monosaccharides from hemicellulose can be carried out in a relatively mild reaction environment, the pH value of the solvent is crucial in generating active oxygen species. In neutral and acidic conditions, the scavenging of h^+ can restrict the conversion of xylose to biomass-derived acid with a lower efficiency. Additionally, carbon nitride modifications have shown excellent performances in the photoreforming of monosaccharides from hemicellulose, indicating the need for more innovative modification strategies and further studies on carbon nitride materials.

6. Photocatalytic decomposition of lignin-model and native lignin

The complicated structure of lignin has evolved over many years and is essential to support the growth of plants in harsh conditions. As mentioned above, lignin is generally composed of three essential elements: coumaryl, conifer and sinapyl alcohol. In general, the structures of lignin in different plants vary and provide various connections based on these three basic units. Lignin monolignols, including a propyl side chain and phenyl group, are linked through C-C and C-O bonds [115]. Dissociating the bonds between these monolignols is an innovative way to extract hydrogen and valuable chemicals through efficient valorization processes. Hydrogen and a range of valuable chemicals can be continuously produced by the valorization steps. Therefore, photoreforming process of lignin has been introduced to replace traditional methods that use critical reaction conditions [116].

6.1. The cleavage of β-O-4 bond in the lignin-model

The complex 3D structure of lignin is primarily composed from C-C and C-O bonds, although the exact structure of lignin is not yet clear, with only knowing that β-aryl ether (β-O-4) is the major linkage in lignin [117]. As a result, the dissociation of C-C and C-O bonds in β-O-4 has been targeted for a long-term to boost the efficiency of depolymerization in lignin. These special bonds have varying bond dissociation energies that connect two benzene rings of lignin [115]. They are C_{ary}-O, C_β-O, C_α-C_β and C_{ary}-C_α in sequence from right side of monolignols to left side, as exhibited in Fig. 4 as the pristine lignin model compound (PP-ol) [118]. Moreover, the oxidation of α carbon atoms in the linkage can efficiently weaken the C-O bond energy by around 14 kcal mol^{-1}, making the cleavage process easier [56,119]. The reduction process with the aid of hydrogen donors, also known as hydrogenolysis, and other special reagents is primarily used for cleaving this bond compared to other methods [115]. Therefore, this distinctive bond is considered one of the most vulnerable points in lignin depolymerization and has prompted numerous approaches to dissociate it recently.

It is feasible to dissociate the C_β-O bond using conventional techniques without catalysts but demanding a large amount of energy inputs under harsh conditions, which can inevitably destroy the benzene rings in lignin. To address this dilemma, researchers have tried to introduce catalysts into the cleavage process at relatively low pressure and temperature to avoid the collapse and destroy of benzene rings. For example, the complex Ru compound-$RuH_2CO(PPh_3)_3$ connected with different ligands was firstly introduced into the C_β-O bond cleavage to provide phenol and acetophenone, as reported by Bergman and Ellman in 2010 [120]. Moreover, a series of other nanomaterials have been utilized for C_β-O bond cleavage, especially when being loaded with Pt, Ru and Pd on the surface [121–123]. However, these reactions are still carried out at high temperatures with rather harsh conditions. Therefore, there is an urgent need to develop photocatalytic cleavage for reforming reactions in mild conditions. Photocatalytic reforming can dissociate the structure of lignin in a mild condition with the low inputs as compared to the chemocatalytic process. Notably, focusing on the dissociation of main linkage (β-O-4) by irradiation can make the photoreforming become possible to produce and collect more value-added products.

6.1.1. Dissociation of β-O-4 linkage via a two-step reaction

The most common approach for the dissociation of C_β-O bond, particularly β-O-4 cleavage, during the photocatalytic process involves two consecutive steps (redox procedure) using different photocatalysts (Fig. 4). Firstly, a selective oxidation reaction of the benzylic β-O-4 alcohol occurs, resulting in the formation of benzylic β-O-4 ketone (**Step 1-blue line**). This step reduces the energy of the C-O bond from 247.9 to 161.1 kJ mol^{-1} [124]. Subsequently, hydrogen from donors reduces the bond, leading to the production of various aromatic monomers after oxidation (**Step 2-brown line**) [125]. Finding an appropriate and effective method to transform the benzylic β-O-4 alcohol into β-O-4 ketone is a top priority for future studies.

A π-conjugated porous organic frameworks (POFs) called carbazolic copolymers (CzCPs) were employed for the photocatalytic decomposition of lignin model compound [125]. It was demonstrated that the oxidative and reductive ability of CzCPs can be controlled by varying the percentage of carbazolic electron donor (D)-DCB and acceptor (A)-4CzIPN. Luo and Zhang demonstrated that CzCP100 (D:A = 0:100) exhibited the highest oxidative ability among the prepared CzCP catalysts and efficiently oxidized the benzylic β-O-4 alcohol to ketone under light irradiation [125]. Control experiments conducted under different conditions yielded an outstanding 100% conversion of benzylic alcohol in the acetone solution with N-hydroxyphthalimide (NHPI) as the hydrogen atom transfer mediator (Table 2). Specifically, the standard conditions of Table 2 were in the presence of 1.5 mol % CzCP100, 15 mol % NHPI (7.5 mg), 0.35 mmol benzylic alcohol (50 μL) and acetone (5

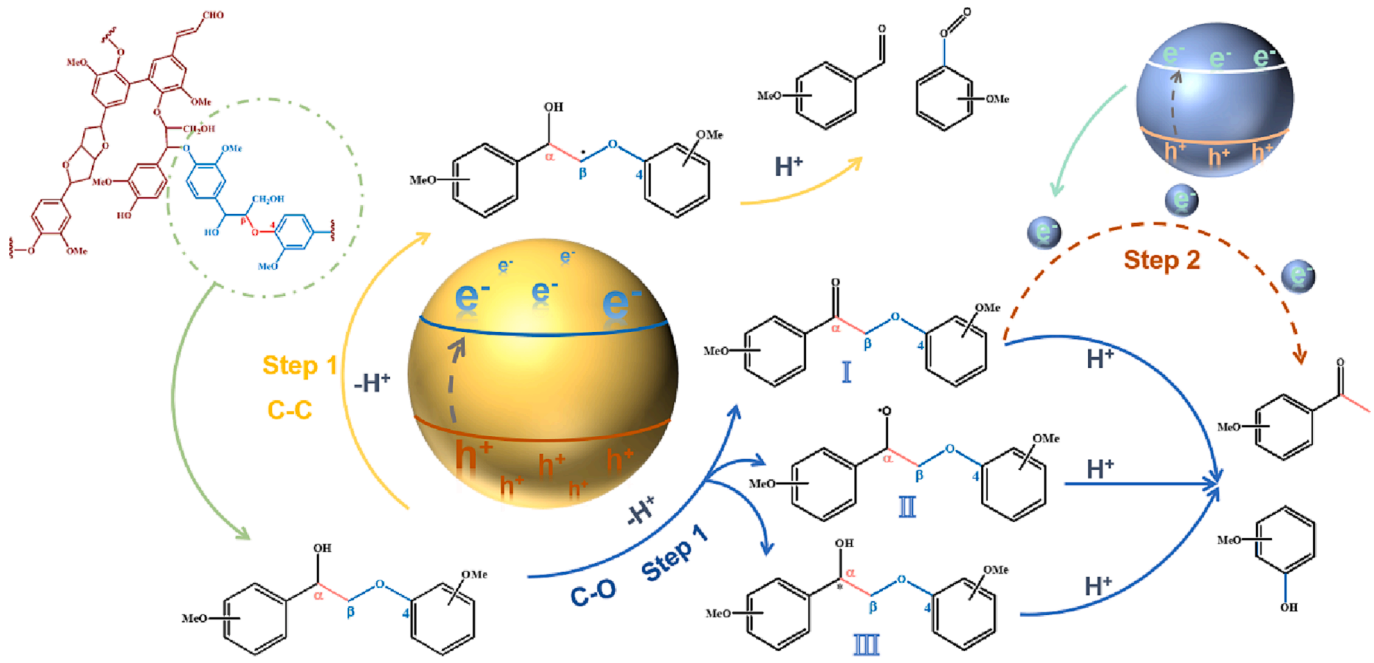

Fig. 4. A proposed mechanism of the C-C and C-O breaking within β-O-4 based on the lignin models (PP-ol).

Table 2
Investigations of photocatalytic oxidation of benzylic alcohol **(1)** [125].

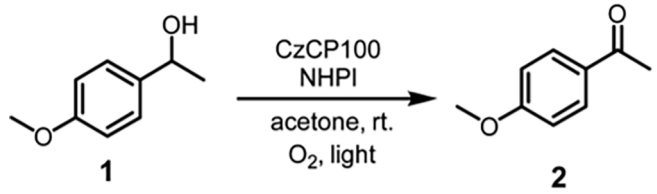

Conditions	Conversion (%)	Yield (%)
Standard conditions	100	99
Without CzCP100	<5	Trace
Without NHPI	15	11
Without O_2	<5	Trace
Acetone/H_2O 9/1 as solvent	100	92

mL), within the oxygen atmosphere (1 atm) under the irradiation from a 26 W compact fluorescent lamp (CFL) at 25 °C for 24 h reaction. The whole conversion results were acquired by ^1H NMR. Notably, this oxidization step can be proceeded at oxygen atmosphere (1 atm) and a normal room temperature.

Following the oxidation step, CzCP33 can efficiently decompose the C-O bond in β-O-4 ketones by reduction reaction, owing to its highest reductive capability. In the presence of formic acid (HCOOH) solution, acetonitrile (MeCN), N,N-diisopropylethylamine (DIPEA), and a light source in an argon atmosphere at room temperature, acetophenone (89% yield) and phenol (86% yield) were the main products. The chemical stability of this nanomaterial was also tested during the oxidation and reduction processes. The oxidation reaction rate of benzylic alcohol over CzCP100 decreased from 98% to 82% after five runs, while the reduction of β-O-4 ketone was performed using CzCP33, and its yield decreased to 75% after 24 h of reaction. Furthermore, this catalyst can be easily collected through centrifugation or filtration, making it promising for practical applications.

Cao et al. investigated and reported another strategy involving two discontinuous steps for photocatalytic C-O bond dissociation in 2-phenoxy-1-phenylethanol (PP-ol) using $CuBr_2$, persulfate, and zinc powders [126]. They found that the in situ EtOH/H_2O/CO_2 can improve the hydrogenolysis via zinc powders after the first photocatalytic oxidation step. This improvement was achieved thanks to the synergy of $CuBr_2$, $(NH_4)_2S_2O_8$ and 1,4-dioxane under normal room temperature for 10 h of irradiation at a wavelength of 475 nm. Furthermore, the impacts of different substituents on the β-O-4 ketone cleavage were also discussed. Electron-withdrawing substituents, such as bromo and chloro, at the para position significantly enhanced the conversion of lignin model compound compared to electron-donating substituents like methyl and methoxy at the same position. As expected, the highest conversion of 2-phenoxy-1-phenylethanone reached 99% in a 2 MPa CO_2 atmosphere and an EtOH-H_2O (2:1) solution over zinc powders.

Stephenson et al. proposed an attractive two-step visible-light lignin degradation perspective for cleaving C-O using a $[Ir(ppy)_2(dtbbpy)]PF_6$. This reaction can be performed under ambient conditions with the presence of N,N-diisopropylethylamine (DIPEA), MeCN and formic acid. The authors demonstrated chemoselective oxidation on the benzylic position in lignin with the synergy of recyclable [4-AcNH-TEMPO]BF_4, DCM (dichloromethane) and silica. This step was followed by a selective reduction cleavage of C-O bonds in lignin models [56]. Table 3 showed high yields of the final products collected when various lignin model substrates were subjected to this system. The yields reported in Table 3 represented an average of two runs and were isolated using column chromatography.

An interesting dual light wavelength switch method was reported by Wang's research team [68]. According to this study, Pd decorated $ZnIn_2S_4$ and TiO_2 were separately subjected to oxidation and reduction by different wavelengths. Then, β-O-4 ketone can be harvested by oxidizing α-C-OH in β-O-4 linkage under illumination at the wavelength of 455 nm on Pd/$ZnIn_2S_4$ (Fig. 4I). Whereafter, the reduction will occur on the surface of TiO_2-NaOAc under illumination with the wavelength of 365 nm to decompose the C-O bond by ethanol (hydrogen donor) (Fig. 4-Step 2). It is noteworthy that the hydrogenolysis of β-O-4 ketones does not exclusively depend on photogenerated electrons from TiO_2. Certainly, Ti^{4+} can trap the photogenerated electrons to produce Ti^{3+} and pass the electrons to β-O-4 ketones, which matched well with the work from Shiraishi [127]. Meanwhile, this theory can be also verified by the work from Feng and Ye in 2018 [128]. A series of noble metals decorated TiO_2 were investigated by the authors to understand the

Table 3
Two-step conversion system of lignin models [56].

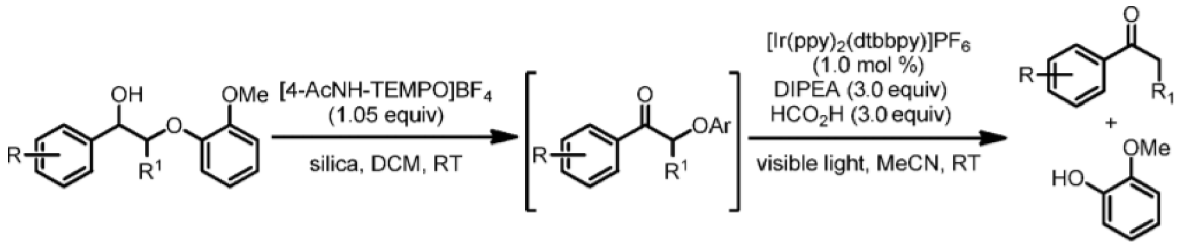

Substrate	Oxid. time (h)	Red. time (h)	Products
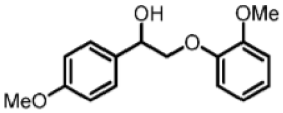	15	16	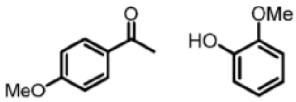
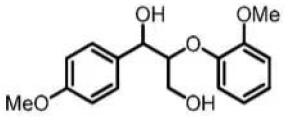	18	20	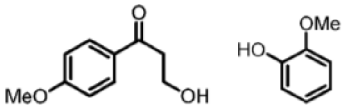
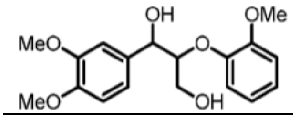	15	14	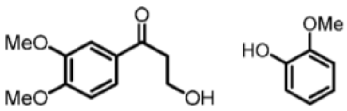

importance of Ti^{3+} rather than the electrons. The conversions in C-O bond dissociation within 2-(2-methoxyphenoxy)-1-(4-methoxyphenyl) ethenone over Ni, Co and Ag decorated TiO_2 were lower than that of pure TiO_2 [128], which indicated that the exposure of active site on bare TiO_2 is the essential factor to promote the reduction process. Notably, based on this two-step system, they speculated a mechanism for the oxidation-hydrogenolysis process. Meanwhile, this system can also work well with the mixed light illumination at 455 and 365 nm, showing a good performance and the yields of phenols can be achieved 97%.

MnO_2 is an another effective catalyst to work for the oxidation step of the lignin model compound such as 1-pheylethanol by the irradiation of blue light [129]. MnO_2 with different phases, for example, α-, β-, γ- and δ-, were employed to oxidize the alcohol into ketone for the further depolymerization of lignin structure. It was found that δ-MnO_2 can offer the best performance than other crystalline types under the light irradiation at the wavelength of 470 nm and oxygen atmosphere. Notably, the oxygen atmosphere is a significant factor for the generation of ketones because O_2^- could efficiently support the alcohol oxidization and prolong the stability of MnO_2 [130]. The collapse in MnO_2 bond will appear, if this kind of oxygen specie releases from the bulk MnO_2 [131,132]. However, in this study, hydrogen can be abstracted and oxidized by oxygen species from alcohol group to emit a acid environment on the surface of δ-MnO_2, which can impede the exposure of O_2^- from δ-MnO_2 to prolong the catalyst stability [133]. Therefore, more metal oxide photocatalysts may provide new perspectives to improve the lignin reformation process.

Moreover, the two-step strategy photocatalytic reforming can bring impressive efficiency to the conversion during the lignin model compound dissociation. However, the redox reaction can hardly take place in a relative complete process in this strategy, which can make the system become tedious, e.g., difficulties in separation and collection of products and catalysts after the reaction. Thus, the integrated step with an exclusive photocatalyst was meaningful to be studied, offering more convenient to promote the reforming.

6.1.2. *Dissociation of β-O-4 linkage via an integrated step*

The two-step strategy for lignin conversion has shown impressive yields, but it can be complex and cumbersome due to the need for different catalysts for each step. As compared with the photocatalytic cleavage of β-O-4 linkages step by step, the sacrificial reductants and oxidants have opportunities to be abandoned in the direct reaction route to save energy [134]. Hence, replacing the tedious two-step system by an integrated one-pot step over the exclusive photocatalyst becomes a hot topic.

A superior C-C bond decomposition strategy (Fig. 4-Step 1) of β-O-4 alcohol was achieved on modified graphitic carbon nitride (mpg-C_3N_4) with a mesoporous structure, synthesized by the modification of urea condensation [135]. In this study, mpg-C_3N_4 was synthesized by modifying urea condensation, while C_3N_4-M and C_3N_4-U were obtained by calcination of melamine and urea, respectively, for comparison. The specific surface area of mpg-C_3N_4 was significantly enhanced to approximately 206 $m^2\ g^{-1}$ with a larger pore size of 3.6 nm, compared to C_3N_4-M (6.6 $m^2\ g^{-1}$) and C_3N_4-U (48.2 $m^2\ g^{-1}$). Meanwhile, various photocatalysts were tested for breaking the β-O-4 linkage of PP-ol to determine the optimal reaction conditions and achieve the highest conversion on mpg-C_3N_4. A remarkable 96% conversion of PP-ol was achieved under 455 nm LED (6 W) irradiation in the presence of O_2, surpassing the conversions obtained with C_3N_4-M (46%) and C_3N_4-U (67%) under the same conditions (Table 4). Notably, acetonitrile was found to be the most efficient solvent for this conversion over mpg-C_3N_4. Other solvents such as CH_3COCH_3, $C_2H_4Cl_2$ and CH_3CH_2OH were also tested but exhibited lower efficiency compared to acetonitrile. Further investigations were carried out using other lignin model substrates with additional methoxy groups. Excellent conversions of these substrates were also achieved over mpg-C_3N_4 under highly efficient conditions using acetonitrile as the solvent and irradiation in an O_2 atmosphere. The proposed mechanism for this process is depicted in Fig. 5, where photogenerated holes and surface basic sites work together to abstract hydrogen from the C_β position, forming the C_β-centered radical (**A**). Furthermore, benzylic alcohol undergoes deprotonation through reaction with $O_2^{\cdot-}$, which results from the reduction of photoexcited electrons with O_2 molecules. These radicals then combine with oxygen and hydrogen to generate a peroxide intermediate. The phenyl formate and aromatic aldehyde were harvested by the clevage of C_α-C_β and O-O bond owing to the migration of electrons within the rings. Additionally, benzoic acid can be obtained through further oxidation of some of the

Table 4
Photocatalytic valorization of 2-phenoxy-1-phenylethanol (PP-ol).

Photocatalyst	Solvent	Mass of Substrate	Light Source	Atmosphere	Irradiation Time (h)	Conversion (%)	Products	Ref.
mpg-C_3N_4 (10 mg)	CH_3CN	0.05 mmol	455 nm LED (6 W)	O_2	10	96	2-phenoxy-1-phenylethanone, benzaldehyde, phenyl formate and benzoic acid	[135]
C_3N_4-M (10 mg)	CH_3CN	0.05 mmol	455 nm LED (6 W)	O_2	10	46	2-phenoxy-1-phenylethanone, benzaldehyde and phenyl formate	[135]
C_3N_4-U (10 mg)	CH_3CN	0.05 mmol	455 nm LED (6 W)	O_2	10	67	2-phenoxy-1-phenylethanone, benzaldehyde, phenyl formate and benzoic acid	[135]
CdS QD-4.4 nm (10 mg)	CH_3CN	0.1 mmol	420-780 nm Xe lamp (300 W)	N_2	3	99	Acetophenone and phenol	[136]
Ag_2S(2%)@CdS (1 mg)	CH_3CN	10 mg	Blue light-emitting diodes LED (6 W)	Ar	3	99	Acetophenone, phenol and 2-phenoxy-1-phenylethanone	[138]
Ni/CdS (20 mg)	CH_3CN/0.1 M KOH (2:8)	5 mM	440-460 nm LED (8 W)	N_2	3	>99	Acetophenone and phenol	[139]
$ZnIn_2S_4$ Sphere-like (5 mg)	CH_3CN	0.1 mmol	455 nm blue LEDs (9.6 W)	Ar	4	>99	Acetophenone, phenol and 2-phenoxy-1-phenylethanone	[50]
$Zn_4In_2S_7$ (10 mg)	CH_3CN/H_2O (1:1)	0.1 mmol	400-780 nm Xe lamp (600 mW cm^{-2})	N_2	4	99	Acetophenone, phenol and 2-phenoxy-1-phenylethanone	[140]

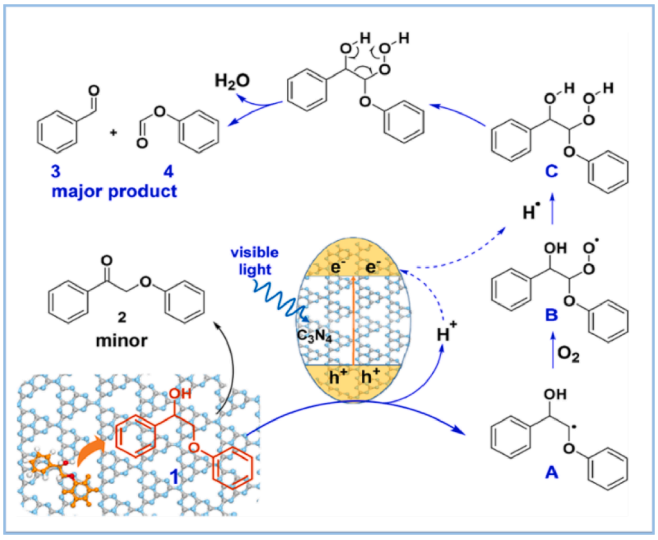

Fig. 5. Illustration of the conversion of 2-phenoxy-1-phenylethanone on mpg-C_3N_4 [135].

aldehyde species.

In addition to modified C_3N_4, there are other photocatalysts that can facilitate the solar-driven conversion of lignin model compounds. For instance, metal-based sulfides like CdS and $ZnIn_2S_4$ have been reported to enable the valorization of native lignin and lignocellulose structures using solar energy. Wu et al. reported that β-O-4 in lignocellulose can be converted into functionalized aromatics while preserving the cellulose and hemicellulose structures through a photocatalytic reaction on cadmium sulphide quantum dots (QDs) [136]. The study employed a simple reversible aggregation-colloidization approach to facilitate easy collection of the catalyst after the reaction. The CdS QDs-MPA, where QDs refer to quantum dots, were prepared by introducing 3-mercaptopropionic acid, a hydrophilic ligand that imparts high solubility to CdS QDs. This ligand-modified catalyst can be easily dispersed in the solution as solubilizing catalysts, eliminating the low efficiency that arises from solid-solid contact within the biomass and heterogeneous phase. Additionally, the catalyst can be easily collected by inducing aggregation with mixing acetone to the reaction solution.

The photocatalytic conversion of PP-ol was carried out in a CH_3CN solution with a series of semiconductors and CdS QDs of varying sizes (Fig. 6**d and e**), under visible and UV-Vis light in the presence of N_2 atmosphere (Fig. 6**a-c**). The highest performance (>90%) in the conversion of PP-ol was observed with CdS QDs having a diameter of 4.4 nm (Fig. 6**b** and Table 4). The conversion occurred via oxidative dehydrogenation (ODH), whereby the holes generated Cα radical intermediates, followed by the reductive dissociation of the β-O-4 linkage with electrons. It is worth noting that CdS QDs not only dissociated the lignin model compounds, but also converted birch woodmeal at room temperature, yielding 27 wt% of functionalized aromatic monomers. Meanwhile, this reaction can also maintain the intact structures of hemicellulose and cellulose.

In addition, the successful depolymerization of native lignin was achieved through the incorporation of CdS QDs and surface ligands. Wang's group investigated the effects of several organic ligands for enhancing the conversion of native lignin [137]. The connection between the organic ligand and the core of CdS QDs had many benefits, including enhanced solubility and electron-transfer (ET) processes. Mercaptoalkanoic acids (MAAs) with different numbers of n in controlling the alkyl-chain lengths, $HS(CH_2)_nCOOH$, have been anchored on the surface of CdS QDs as the mediates of electron-transfer. The experiments adopted three different n values (2, 5, 10), and the samples derived from these values were named CdS-C3, CdS-C6 and CdS-C11 in sequence (Fig. 7**a**). The best performance in the reformation of native lignin, 27 wt%, was achieved with CdS-C3 under ambient conditions and visible light irradiation (Fig. 7**b**). The photoelectrochemical characterizations were proceeded on the lignin model compound solution (PP-ol), simulating the real lignin structure (Fig. 7**c-f**). The shortest length of ligand on the surface of CdS-C_x QDs easily offered the highest photocurrent upon light exposure, and this result was consistent with the tendency observed from linear sweep voltammetry. The electrochemical impedance spectra displayed that the ability of charge-transfer was lowest when the length of alkyl chain was prolonged. These phenomena indicated that the ligand was a significant factor in the charge transformation between the core of CdS QDs and the targeted biomass. The electron-hole coupled (ECHO) photoredox mechanism was used to describe and exhibit the lignin conversion process in a previous work. In this mechanism, oxidative dehydrogenation generates a C_α radical and proton through the reaction between photogenerated holes and reactant (Fig. 4III). The bond dissociation energy (BDE, 7.8 kcal mol^{-1}) of β-O-4 in the C_α intermediate is lower than the BDE (55 kcal mol^{-1}) in PP-ol structure. The electrons will be transferred by the ligand from the core of CdS QDs to participate the next step, producing acetophenone and

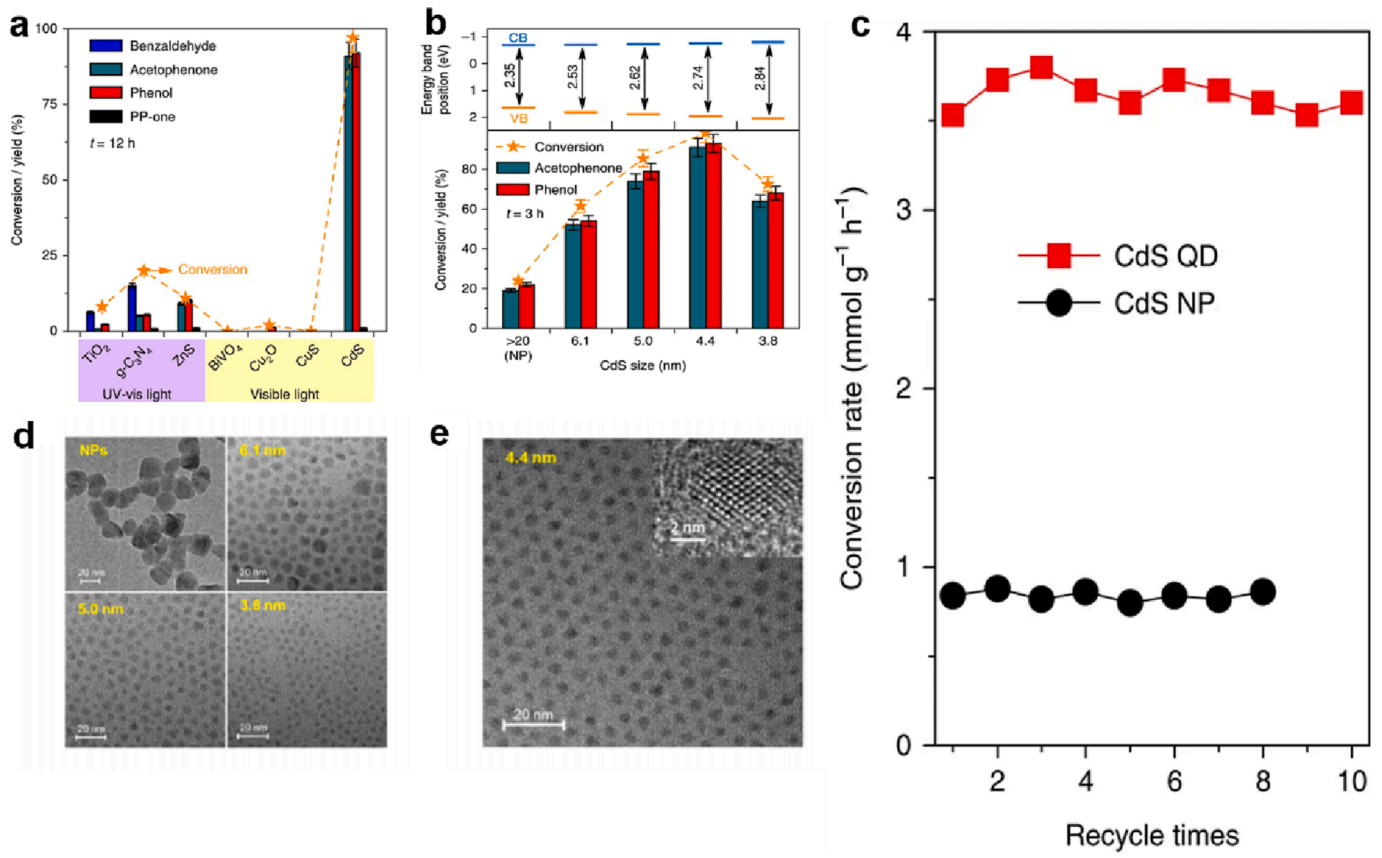

Fig. 6. The photocatalytic dissociation of β-O-4 linkage within lignin model substances. (a) Photoreforming of PP-ol with different nanomaterials. (b) The relation between the potisionts of energy-band and various diameters of CdS regarding photocatalytic performances. (c) The conversion of PP-ol based on the reuse of CdS QD-4.4 nm and CdS NPs. (d) TEM micrographs of CdS NPs and CdS QDs with sizes of 6.1, 5.0 and 3.8 nm. (e) TEM and HRTEM micrographs of 4.4 nm CdS QDs [136].

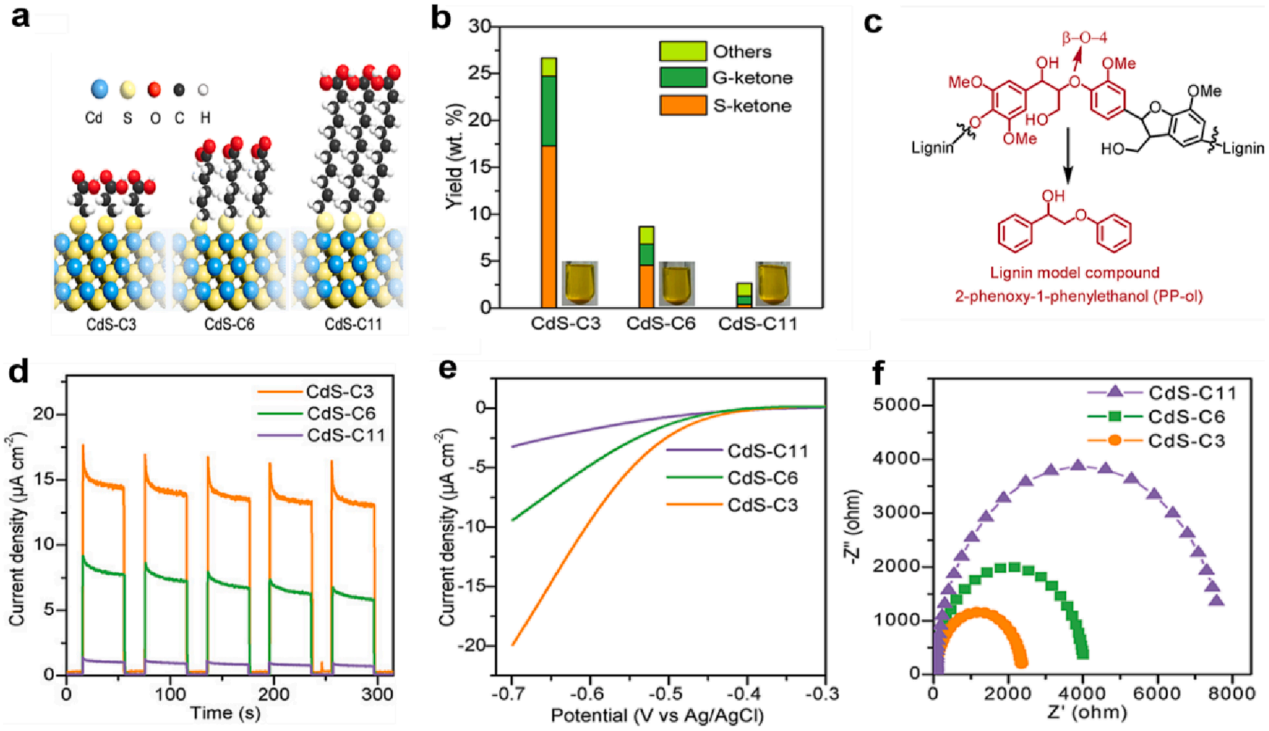

Fig. 7. Illustration for the catalytic activities of CdS-Cx QDs within the conversions of native lignin. (a) Illustration of the differences between three types of CdS-Cx QDs. (b) Aromatic monomers yield by CdS-Cx QDs. (c) Schematic structure of the lignin fragment. (d) Photocurrent spectra. (e) Linear sweep voltammetry spectra. (f) EIS results [137].

phenoxy anion. Finally, the proton can be accepted by phenoxy anion to generate phenol. Therefore, modifying the ligand can increase the efficiency of breaking the β-O-4 linkage.

Besides, another highly efficient CdS based catalyst, Ag^+-exchanged CdS, was prepared via a facile vigorous stirring in the mixture of Ag^+ solution and dispersed CdS nanoparticles [138]. Ag^+ can substitute Cd^{2+} to induce Ag_2S on the surface of pristine CdS, and the resulting sample shows higher photocatalytic ability than pure CdS. The Fermi level migrated to the VB due to the support of Ag^+, accelerating the reductive cleavage on β-O-4 via electrons transfer in the CB rather than accumulation. Meanwhile, the recombination of photoexcited electron-hole can be restrained because of the growth in the state of Ag^+ exchange. The binding energy of sulfur was toward the negative values, resulting in a growth in the H^+ affinity of sulfide ions on this photocatalyst for forming the active site. Consequently, β-O-4 of PP-ol can be easily dissociated by the abstracted H^+ and electrons after the dehydrogenation by holes. Therefore, the highest conversion of PP-ol can be collected by Ag_2S(2%) @CdS compared with other metal sulfide photocatalysts.

To promote the efficiency in the photocatalytic depolymerization process, a variety of transition metals (Mn, Ni, Co, Cu, and Fe) were reduced and decorated on the ultrathin CdS nanosheet by the reduction over $NaBH_4$ and their metal chloride salts [139]. Ni decorated CdS was found to provide the highest performance in dissociating the β-O-4 bond through the cooperation of CH_3CN and KOH. The mixed solvent of CH_3CN/H_2O (volume ration is 2:8) and KOH (0.1 M) make the absorbed hydrogen species preferably move to the β-O-4 linkage, generating phenol and acetophenone. The thin layer of NiO_x or $Ni(OH)_2$ was bred by the additional alkaline condition, promoting the migration of absorbed hydrogen species to C_β-O bond because the hydrogen evolution reaction is hard to be carried out on these oxidized nickel compounds.

Another sphere-like sulfide catalyst, $ZnIn_2S_4$, with a size of 0.5-6 μm, was introduced to dissociate the β-O-4 linkage through the catalytic transfer hydrogenation (CTH) over the proton from the oxidized substrate (Fig. 8**a-e**) [50]. The mapping results can support the successful synthesis of the catalyst (Fig. 8**f**). A 'hydrogen pool' was created on the surface of $ZnIn_2S_4$ due to the aggregation of protons. Different solvents and atmospheres were chosen to work with $ZnIn_2S_4$ under 9.6 W blue LEDs light for optimizing the best condition to convert the PP-ol. It was also found that the source of hydrogen from the solvent and gas was not the exclusively dependent factor for the hydrogenolysis. The conversion driven by Ar and H_2 atmosphere in the fragmentation of PP-ol was similar, while $ZnIn_2S_4$ was working in the same condition such as CH_3CN solution, 9.6 W blue LEDs (455 nm) and 42 °C (Table 4). Besides, three different solutions including THF, acetone and ethanol were respectively introduced into the reaction to differentiate the effect of hydrogen-donor solution during the hydrogenolysis. The yields of acetophenone and phenol reached 95 and 96% in the ethanol solution, respectively. According to the results, the dissociation of PP-ol in the ethanol solution was similar to the reactions in THF and acetone, proving that the hydrogen-donor solvents were not essential in this system.

It has been concluded that $ZnIn_2S_4$ is capable of promoting the hydrogenolysis of lignin through a self-hydrogen transfer mechanism. This was demonstrated by the catalysis of dioxanesolv poplar lignin to produce a 67% yield of p-hydroxylacetophenone in a solution of acetone and isopropanol. The depolymerization of lignin and its models were all established on the mechanism predicted by the time-on-course process over PP-ol. In this process, the lignin model compound was initially oxidized by photoinduced holes, releasing the radicals after the H-abstraction of α-OH groups. Subsequently, a 5-6% yield of 2-phenoxy-1-phenylethanone was obtained through the H-abstraction of α-CH. Protons, which were generated from the oxidization of abstracted H and holes, would be absorbed by the catalyst, creating a 'hydrogen pool'. The final products, acetophenone and phenol, will be produced by cleaving C_β-O bond via the reaction of 2-phenoxy-1-phenylethanone and 'hydrogen pool' (Fig. 4 II).

Furthermore, a series of $Zn_mIn_2S_{m+3}$ (m = 1, 2, 3, 4, 5, 6) were prepared via a facile hydrothermal approach (low-temperature) for understanding the mechanism in the β-O-4 bond dissociation process (Fig. 9**a**). The multi-layered structure was proven by the images of TEM and HRTEM of $Zn_4In_2S_7$ in Fig. 9**b-j**. Also, the crystallographic plane (102) matched well with the interplanar spacing of 0.32 nm. As depicted in Fig. 9**k-m**, the increase of band-gap energy can be varied by the incremental atomic scale of S, In and Zn, shifting to the shorter wavelength of absorption edge. Notably, $Zn_4In_2S_7$ can provide the highest conversion of PP-ol under a 4-h visible light illumination due to its competitive physicochemical property (Table 4). A more plausible mechanism was proposed in this work over $Zn_4In_2S_7$ [50,136]. This mechanism was established by the cleavage of C_α-H to C_α radical, which can weaken the bonding energy of β-O-4 from 55 to 7.8 kcal mol^{-1}. This mechanism is similar to that proposed in previous work on CdS QDs (Fig. 4III) [136]. There was no doubt that the key factor was the selectivity of cleavage in benzylic C_α-H bond during the major pathway. It can conclude that thiyl radicals can be generated by the oxidation of the surface groups, -SH, to generate C_α radical intermediate, preparing for the further dissociation of β-O-4 linkage. These thiol groups could drive the C-H activation as the active centre on the surface of sulfide catalysts. Therefore, it was possible to achieve a yield of 18.4 wt% by the conversion of organosolv

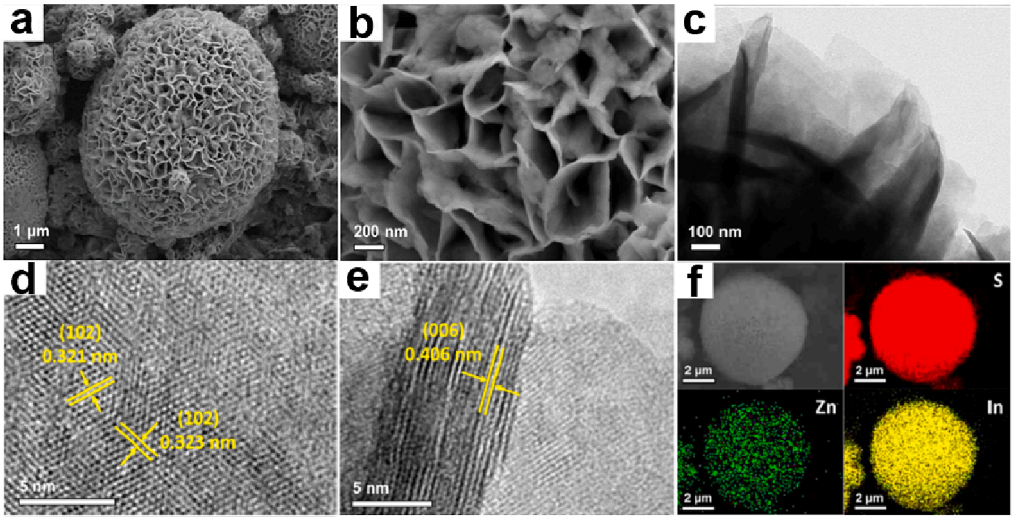

Fig. 8. Morphology of $ZnIn_2S_4$. (a-b) SEM images. (c) TEM image. (d-e) HRTEM images. (f) Element mappings [50].

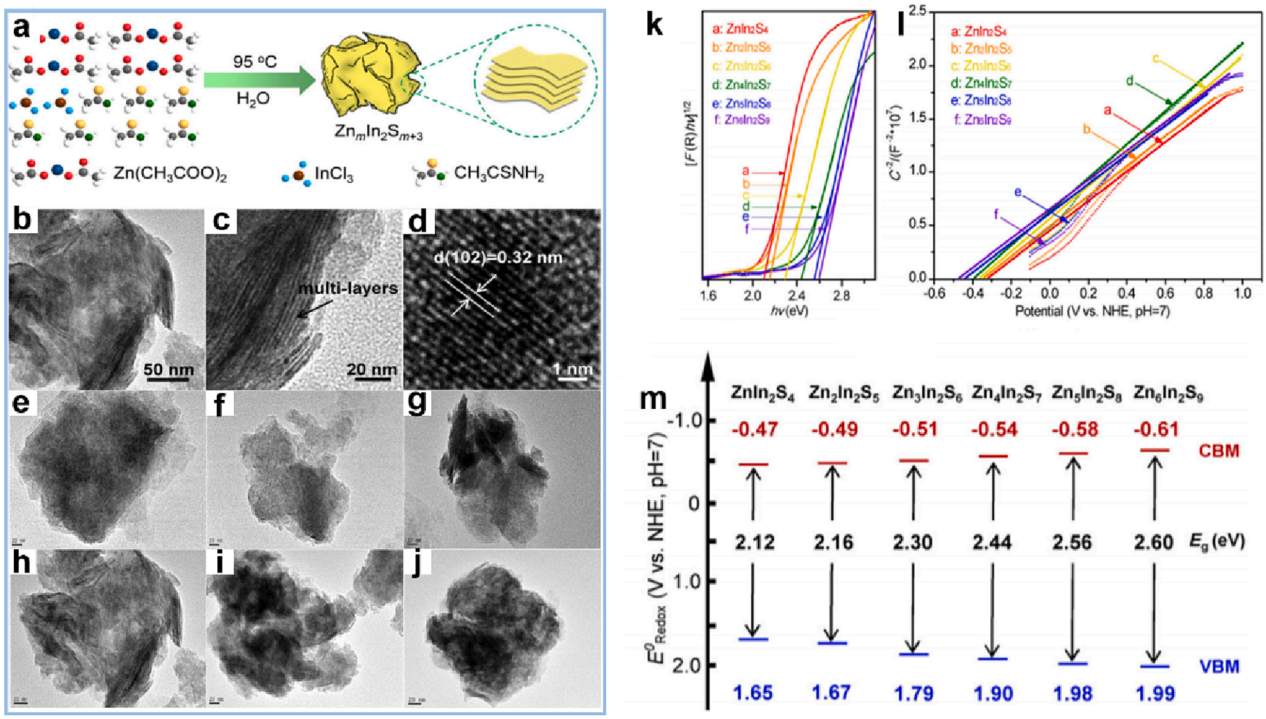

Fig. 9. (a) Schematic synthesis of $Zn_mIn_2S_{m+3}$ (m = 1, 2, 3, 4, 5, 6) photocatalysts. (b-d) Images of TEM and HRTEM on $Zn_4In_2S_7$. (e-j) TEM images of $Zn_mIn_2S_{m+3}$ samples. (k) The spectra of modified Kubelka-Munk function versus the energy of exciting light of prepared materials. (l) The spectra of Mott-Schottky and (m) band structure of $Zn_mIn_2S_{m+3}$ [140].

birch lignin over $Zn_4In_2S_7$ with the support of -SH under visible light irradiations.

According to the studies above, most of integrated step approaches can be proceeded by modified C_3N_4, binary (CdS) and multinary sulfides ($Zn_mIn_2S_{m+3}$). It is worth noting that modified transition metal sulfides, CdS and $Zn_mIn_2S_{m+3}$, can provide better performances of conversion of PP-ol than modified C_3N_4 in the short period of irradiation. Specifically, the preparation of multinary sulfides ($Zn_mIn_2S_{m+3}$) can give few creative ideas to modify the chalcogenide because the incorporation of cation in binary sulfides (ZnS) can narrow the bandgap, obtaining a wide spectrum responding ability. Meanwhile, a reasonable change in the composition and stoichiometry can also vary the band structure to tune the redox potentials. All the modifications can make these catalysts exhibit high performances in the real lignin valorization system.

6.2. Photocatalytic dissociation of β-5 linkage

The photocatalytic dissociation of β-O-4 linkage has been extensively studied, while the studies on the photoreforming of β-5 linkage has been rarely explored and reported. β-O-4 linkage accounts for only 45-50% of lignin, while β-5 and 5-5′ biphenyl comprise 9-12% and 19-22%, respectively, in softwood species [141]. Therefore, exploring photocatalytic reforming of β-5 and 5-5′ biphenyl is important to acquire a deeper insight of the photoreforming of lignin. Recently, it is noteworthy that the photocatalytic dissociation of the β-5 model dimer was firstly reported by TiO_2 (P25/P20) with UV-LED [142]. The β-5 linkage can be completely dissociated in 45 min irradiation with the degradation rate (0.0063 mg ml^{-1} min^{-1}) in the mixture of H_2O and CH_3CN (1:1). This pioneering study on the photocatalytic conversion of β-5 linkage offers a new direction for investigating the photoreforming of lignin.

6.3. Photocatalytic hydrogen evolution in lignin reforming process

Monitoring hydrogen evolution from biomass substrates is another significant indicator to express the efficiency in photoreforming. As shown in the previous reports, metal sulfide photocatalysts can work well in dissociating the β-O-4 bond. Therefore, CdS, a metal sulfide photocatalyst, was investigated for hydrogen collection by reforming lignin substrates due to its outstanding properties in bond dissociation of the lignin structure under visible light irradiations. CdS has appropriate conduction band (CB) and valence band (VB) energy levels (-0.5 eV and 1.9 eV, respectively) versus the normal hydrogen electrode (NHE), which can facilitate proton reduction and saccharide oxidation [143,144].

Recently, Wakerley et al. prepared ligand-free CdS quantum dots (QDs) with a size of 5 nm (Fig. 10**a and b**) covered by a monolayer and a few layers of CdO_x ($Cd(OH)_2$ and CdO) shell in a high concentration alkaline solution [20]. The surface of CdS QDs were passivated by N, N-dimethylformamide and tetrafluoroborate anions which can easily allow OH^- to connect to the surface sites of Cd in the basic solution. Besides, Cd-O^- can be created on the surface of CdS QDs with the decline in an average particle size of 0.6 nm after the isolation from KOH (10 M) (Fig. 10**c and d**). They also observed a decrease in surface charge with an increase in pH value above 12, which is consistent with the previous observation on $ZnS/Zn(OH)_2$ [145]. These phenomena can demonstrate that Cd-O^- formed on the particle surface. The shell is thin enough to allow the mobility of photoexcited electron-hole from core to the solution (Fig. 10**e**). Meanwhile, the photocorrosion is suppressed as well during the photocatalytic reaction.

The lignocellulose and a variety of raw biomass were introduced into the photoreforming reaction in the alkaline solution using CdS/CdO_x and $Co(BF_4)_2$ cocatalysts, showing impressive performances in hydrogen generation. The higher reformation rates were found for cellulose and hemicellulose because of their similar chemical compositions. Also, the higher H_2 generation can be ascribed to the better solubility of hemicellulose than cellulose. On the contrary, the reformation of lignin was with the lowest hydrogen evolution rate (0.26 mmol $g_{cat}^{-1}h^{-1}$), compared with the rates of hemicellulose and cellulose due to its stubborn structure and strong light-absorbing ability, making it challenging to study its oxidation-driven hydrogen release [63,146]. Nevertheless, a remarkable

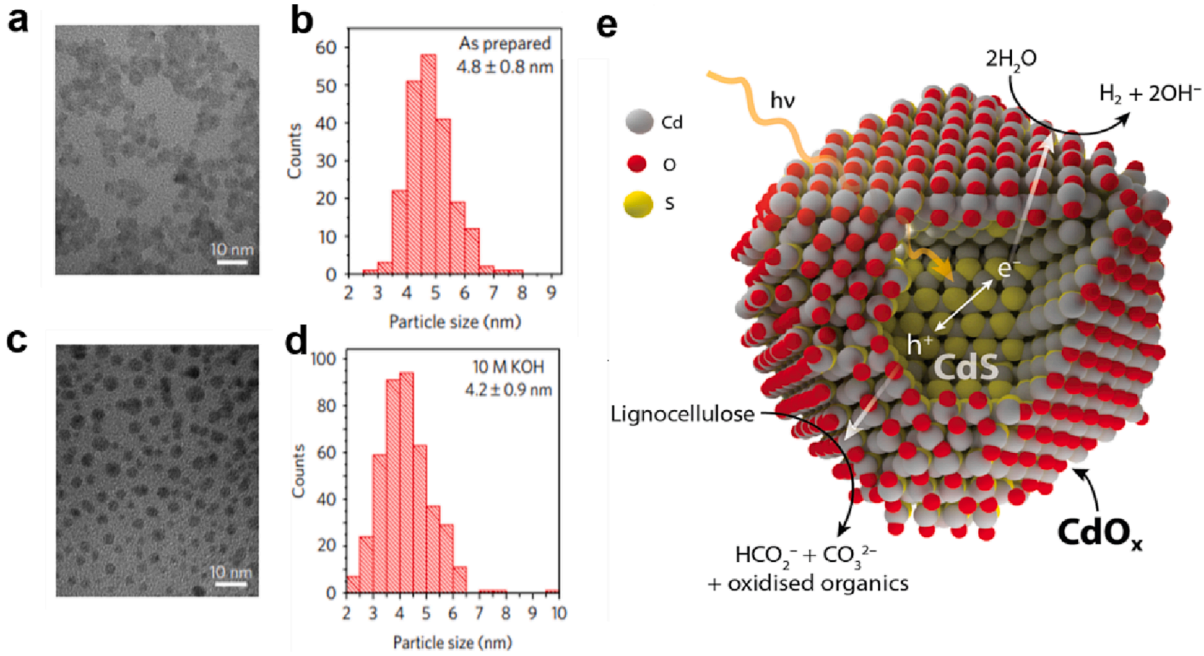

Fig. 10. (a) TEM image for ligand-free CdS QDs. (b) Size distribution of CdS QDs. (c) Morphology of CdS/CdO_x after collection from KOH solution (10 M). (d) Size distribution of CdS/CdO_x catalysts. (e) Schematic illustration of H_2 evolution from the photocatalytic reformation of lignocellulose over CdS QDs [20].

hydrogen generation rate of wooden branches was observed (5.59 mmol $g_{cat}^{-1}h^{-1}$) (Table 5) in this catalytic system owing to the high pH reaction environment. The alkoxide groups formed when substrates were bonded on the surface of CdO_x. Meanwhile, the lignocellulose and raw biomass were connected to CdS/CdO_x by Cd-O-R bonds. This bond was similar as Ti-O-R, which can promote the formation of decarboxylation substance, CO_3^{2-}. Thus, Cd-O-R can facilitate the migration of holes to oxidize the lignocellulose to receive aldehydes and cleave the C-C bond, producing the hydrogen in an efficient pathway.

In addition to 0D CdS QDs, 1D CdS coated by NiS particles can also reform the lignin in an efficient way for the hydrogen collection. Those NiS particles can be tightly deposited on the CdS nanowire, reinforcing the separation of photoexcited electron-hole. Hence, 0.2-NiS/CdS displayed the highest hydrogen evolution rate (1.512 mmol $g_{cat}^{-1}h^{-1}$) when irradiated with visible light and using a mixture of lignin and lactic acid (Table 5) [147]. Additionally, the spectra of UV-Vis showed that the degradation of lignin took place with the gradually decreasing absorption intensity at approximately 210 nm, which is in accordance with the unsaturated chains in lignin structure [146]. This result can demonstrate the decomposition of lignin. Specially, 0.2-NiS/CdS showed the distinguished activity both in the hydrogen generation and lignin decomposed process because of the longer charger carrier lifetime among all the NiS modified CdS. The hydrogen may came from the contribution of by-products, e.g., oxalic acid, formic acid, ethanol, methanol and formaldehyde, derived from the decomposition of lignin [148].

Modified carbon nitride is another excellent photocatalyst candidate to oxidize the lignocellulose biomass by holes to release hydrogen. It was reported that mesoporous mpg-C_3N_4 can efficiently decompose the lignin model structure with a 96% conversion of PP-ol under the 455 nm LED (6 W) irradiations in the previous study [135]. It was concluded that the engineered carbon nitride can show a high performance in the hydrogen evolution during the dissociation of lignocellulose biomass. After that, cyanamide-functionalized $^{NCN}CN_x$ was synthesized to efficiently oxidize the substrates after the activation in the potassium phosphate (KP_i) solution by sonication [149]. The pristine $^{H2N}CN_x$, bulk $^{NCN}CN_x$ and activated $^{NCN}CN_x$ were compared with the α-cellulose reformation process in the same reaction condition, i.e., 3 mL KP_i solution (0.1 M and pH = 4.5), as shown in Fig. 11**a**. The best performance is found to be the activated $^{NCN}CN_x$ rather than pristine $^{H2N}CN_x$ and bulk $^{NCN}CN_x$. Activated $^{NCN}CN_x$ possessed a smaller aggregate size, and enlarged surface area by the sonication process (Fig. 11**d and e**). Furthermore, the activation process provided a higher surface area than the bulk $^{NCN}CN_x$, which is 97.4 ± 0.6 m^2 g^{-1}. The volume of activated $^{NCN}CN_x$ is higher than the bulk one at the same weight (Fig. 11**f**). Therefore, more active sites can be acquired by a large surface area on the photocatalysts to drive the oxidization of xylan, α-cellulose, lignin and raw biomass substrates become real, releasing the hydrogen under irradiations from visible light as in Fig. 11**b and c**. As such, the hydrogen generation rate (0.015 mmol $g_{cat}^{-1}h^{-1}$) of lignin is shown in Table 5. Notably, the organic substrates were dispersed and stirred in KOH (10 M) at room temperature for 24 h before the reaction in Fig. 11**c**.

Based on the studies discussed above, it has been shown that both C_3N_4 and chalcogenide materials are effective in bond dissociation and hydrogen evolution from the reforming of lignin. As such, among the

Table 5
Photocatalytic hydrogen production in the reforming process of biomass.

Photocatalyst	Solvent	Substrate	Light Source	Atmosphere	Illumination Time (h)	Hydrogen Generation (mmol $g_{cat}^{-1}h^{-1}$)	Ref.
CdS/CdO_x (0.5 μM)	KOH solution (25 °C) with $Co(BF_4)_2$	Wooden branch	100 mW cm^{-2}	N_2 and 2% CH_4	24	5.59	[20]
0.2-NiS/CdS (100 mg)	Aqueous solution	Lignin and lactic acid	Xe lamp (300 W)	Vacuum	3	1.512	[147]
Activated $^{NCN}CN_x$ (5 mg)	KOH solution (25 °C)	Lignin	Xe lamp (100 mW cm^{-2})	N_2 and 2% CH_4	288	0.015	[149]

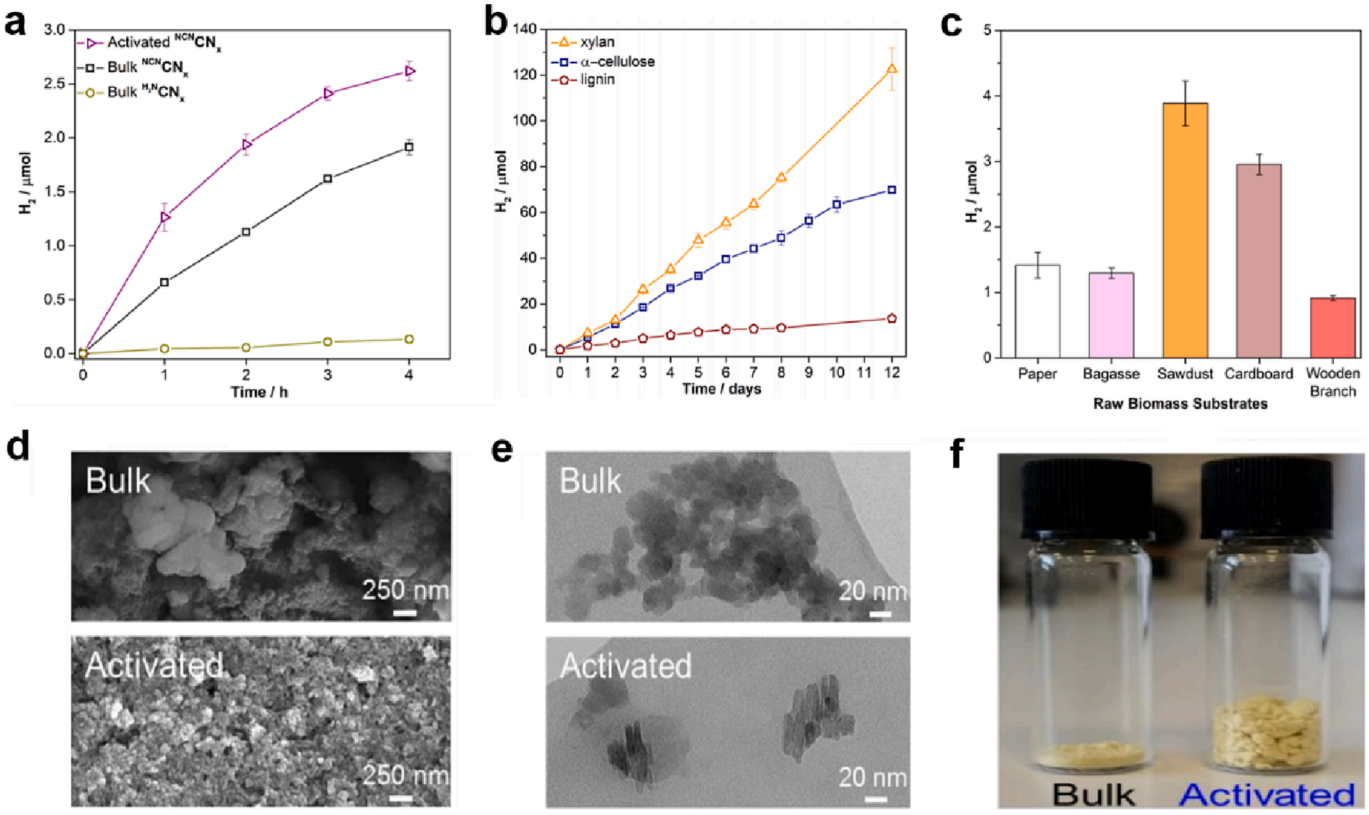

Fig. 11. (a) Photocatalytic H_2 generation over 5 mg bulk $^{H2N}CN_x$, activated and bulk $^{NCN}CN_x$, 50 nmol NiP with 100 mg α-cellulose. (b) 5 mg activated $^{NCN}CN_x$ with 4 wt% H_2PtCl_6 and 100 mg cellulose, 50 mg xylan, 0.5 mg lignin in 3 mL KOH solution (10 M and pH = 15) for 12 days. (c) 5 mg activated $^{NCN}CN_x$ and 50 nmol NiP with 100 mg raw biomass compounds in 3 mL KP_i solution (0.1 M and pH = 4.5) for 24 h illumination. (d) SEM and (e) TEM of bulk and activated $^{NCN}CN_x$. (f) Volume comparison of 20 mg activated and bulk $^{NCN}CN_x$. Note: the intensity of the simulated solar energy is 100 mW cm^{-2} at room temperature (AM1.5G) [149].

chalcogenide materials, CdS/CdO_x and 0.2-NiS/CdS exhibited more promising performances in hydrogen production compared to modified C_3N_4. In fact, many studies have demonstrated excellent results achieved through a variety of modified metal sulfides, suggesting the great potential of sulfides in this field. While most metal sulfides can show excellent performances in the short period reaction, their performances always decline in the long-term photocatalysis. This is because of the main chronic drawback of metal sulfides, which is the instability due to photocorrosion. Hence, finding innovative strategies to prolong the lifetime of metal sulfides should become the primary focus in future research.

7. Conclusions and perspectives

Converting renewable biomass into valuable chemicals and fuels by solar energy holds a great promise for future energy sustainability. This review presents the latest advances in photocatalytic reforming of glucose, lignocellulose, and their model compounds. With the comparison of the variety of valorizations in this review, photocatalytic conversion of biomass is demonstrated to possess impressive performances. However, most investigations have been limited to laboratory scale due to the low efficiency compared to conventional processes. To realize practical-scale photoreforming of biomass, two essential factors are highlighted: i) controlling the redox potentials of photocatalysts to improve the bond cleavage efficiency, and ii) using different solvents with various pH values to enhance the solubility of biomass and optical properties of photocatalysts. It is noteworthy that metal sulfides, e.g., CdS, NiS, Ag_2S and $Zn_mIn_2S_{m+3}$, can support most of the photocatalytic biomass conversions through the breakage of C-O and C-C bonds. The redox potentials of these chalcogenide materials can be tuned and modified to harvest the desired selectivity in the photocatalytic cleavage of biomass. Besides, the different solvents and pH values can also reinforce the photocatalytic properties of metal sulfides, for instance, the high concentration of -OH can provide a hydroxide or oxide (CdO_x/Cd$(OH)_2$) cover the surface of CdS. Thus, by following these essential factors, it may be possible to introduce photocatalytic reforming of biomass into the commercial stage.

According to the studies in this review, converting biomass to valuable chemicals and clean fuels by solar energy contains a huge potential to replace the conventional chemocatalytic process. However, some critical issues regarding photocatalysts and solvents are still existing in the photocatalytic reforming even when the redox potential is fulfilled. Notably, three basic properties of photocatalysts, e.g., stability, toxicity and recoverability, always are the first mission to be considered and discussed. The excellent merits of photocatalysts can attract attention via the high selectivity of the biomass cleavage (C-O and C-C bonds) and the generation of hydrogen, but not all the materials can successfully avoid the photocorrosion. Based on the previous studies, a considerable of metal sulfides were introduced into the photoreforming systems, showing attractive performances as the typical highly efficient photocatalysts. Nonetheless, they are more toxic and unstable than other photocatalysts such as metal oxide because S^{2-} is easily to be oxidized, collapsing the structure of themselves during redox reaction. Metal sulfides can also unconsciously introduce the difficulties to purification and recovery procedures. On the contrary, modified carbon nitride, as a typical metal free nanomaterial, can overcome the shortcomings from metal sulfide because they are friendly to environment and more stable. This material has the prospect to be investigated in bond dissociation though a few reports work with them right now. Thus, finding a balance between merits and disadvantages among these two efficient materials will be focused in the future studies.

Besides, another important factor should be carefully treated and

considered is the choice of solvent. Most of previous reports show that the acetonitrile and basic solution can support the photoreforming by enhancing the solubility of biomass in the solution, leading to the difficulties in the purification. This is because different final products and raw biomass in these solvents will show the distinct polarities. Based on this dilemma, the future efforts should be moved to design the most cost-effective plan to separate and purify the solutes, solvents and photocatalysts after the reaction via a facile step.

Moreover, the following three critical concepts should be addressed to realize the feasibility of photoreforming at the industrial scale: 1) Various visible-light-driven photocatalysts were successfully employed in the photoreforming reactions. Nonetheless, the poor selectivity and efficiency in the biomass conversion performance always exist. Thus, modifying the physiochemical properties, e.g., crystal and space structure, surface states and chemical composition, should be investigated to achieve the utilization of full solar energy and charge mobility to reduce the charge recombination. 2) The specific mechanisms of photocatalytic reforming on native lignin still cannot be clearly explained. Thus, controlling pathways of lignin conversion process is another challenge. To overcome this challenge, in situ technologies, e.g., in situ NMR spectroscopy, Raman and FT-IR, can be employed in the photoreforming of native lignin to illustrate the reaction pathways. 3) A variety of pretreatment processes of lignin could introduce the variations in their purity and structure. These random and irregular properties can hinder the efficiency of photocatalysts. In the meantime, the photocatalytic conditions are also impacted by these properties. As such, the interaction of different views via not only photocatalysis, but other scientific fields are also a feasible and valuable orientation to be considered in the future work. The integration may have a potential to convert native biomass into the desired products efficiently.

Declaration of Competing Interest

The authors declare that they have no known competing financial interests or personal relationships that could have appeared to influence the work reported in this paper.

Data availability

No data was used for the research described in the article.

References

[1] H. Song, S. Luo, H. Huang, B. Deng, J. Ye, Solar-driven hydrogen production: Recent advances, challenges, and future perspectives, ACS Energy Lett. 7 (2022) 1043–1065.

[2] Y. Li, L. Yang, H. He, L. Sun, H. Wang, X. Fang, Y. Zhao, D. Zheng, Y. Qi, Z. Li, W. Deng, In situ photodeposition of platinum clusters on a covalent organic framework for photocatalytic hydrogen production, Nat. Commun. 13 (2022) 1355.

[3] T. Takata, J. Jiang, Y. Sakata, M. Nakabayashi, N. Shibata, V. Nandal, K. Seki, T. Hisatomi, K. Domen, Photocatalytic water splitting with a quantum efficiency of almost unity, Nature 581 (7809) (2020) 411–414.

[4] S. Guo, X. Li, J. Li, B. Wei, Boosting photocatalytic hydrogen production from water by photothermally induced biphase systems, Nat. Commun. 12 (2021) 1343.

[5] C.R. López, E.P. Melián, J.A. Ortega Méndez, D.E. Santiago, J.M. Doña Rodríguez, O. González Díaz, Comparative study of alcohols as sacrificial agents in H_2 production by heterogeneous photocatalysis using Pt/TiO_2 catalysts, J. Photochem. Photobiol., A 312 (2015) 45–54.

[6] K.A. Davis, S. Yoo, E.W. Shuler, B.D. Sherman, S. Lee, G. Leem, Photocatalytic hydrogen evolution from biomass conversion, Nano Converg. 8 (2021) 6.

[7] R.M. Navarro, M.C. Sánchez-Sánchez, M.C. Alvarez-Galvan, F.D. Valle, J.L. G. Fierro, Hydrogen production from renewable sources: biomass and photocatalytic opportunities, Energy Environ. Sci. 2 (1) (2009) 35–54.

[8] A. Fujishima, K. Honda, Electrochemical photolysis of water at a semiconductor electrode, Nature 238 (5358) (1972) 37–38.

[9] Y. Lin, W. Su, X. Wang, X. Fu, X. Wang, LaOCl-coupled polymeric carbon nitride for overall water splitting through a one-photon excitation pathway, Angew. Chem. Int. Ed. 59 (47) (2020) 20919–20923.

[10] T. Kawai, T. Sakata, Photocatalytic hydrogen production from liquid methanol and water, J. Chem. Soc., Chem. Commun. (1980) 694–695.

[11] T. Kawai, T. Sakata, Conversion of carbohydrate into hydrogen fuel by a photocatalytic process, Nature 286 (5772) (1980) 474–476.

[12] A. Gallo, T. Montini, M. Marelli, A. Minguzzi, V. Gombac, R. Psaro, P. Fornasiero, V. DallSanto, H_2 production by renewables photoreforming on $Pt–Au/TiO_2$ catalysts activated by reduction, ChemSusChem 5 (9) (2012) 1800–1811.

[13] E. Lam, M. Miller, S. Linley, R.R. Manuel, I.A.C. Pereira, E. Reisner, Simultaneous conversion of CO_2 and cellulose to formate using a floating TiO_2-enzyme photoreforming catalyst, Angew. Chem. Int. Ed. (2023), e202215894.

[14] C.K. Prier, D.A. Rankic, D.W.C. MacMillan, Visible light photoredox catalysis with transition metal complexes: applications in organic synthesis, Chem. Rev. 113 (2013) 5322–5363.

[15] J.M.R. Narayanam, C.R.J. Stephenson, Visible light photoredox catalysis: applications in organic synthesis, Chem. Soc. Rev. 40 (2011) 102–113.

[16] K. Kalyanasundaram, Photophysics, photochemistry and solar energy conversion with tris(bipyridyl)ruthenium(II) and its analogues, Coord. Chem. Rev. 46 (1982) 159–244.

[17] S. Bhattacharjee, V. Andrei, C. Pornrungroj, M. Rahaman, C.M. Pichler, E. Reisner, Reforming of soluble biomass and plastic derived waste using a bias-free $Cu_{30}Pd_{70}$|perovskite|Pt photoelectrochemical device, Adv. Funct. Mater. 32 (2022) 2109313.

[18] R.A. Sheldon, Green and sustainable manufacture of chemicals from biomass: State of the art, Green Chem. 16 (3) (2014) 950–963.

[19] H. Nagakawa, M. Nagata, Photoreforming of lignocellulosic biomass into hydrogen under sunlight in the presence of thermally radiative CdS/SiC composite photocatalyst, ACS Appl. Energy Mater. 4 (2) (2021) 1059–1062.

[20] D.W. Wakerley, M.F. Kuehnel, K.L. Orchard, K.H. Ly, T.E. Rosser, E. Reisner, Solar-driven reforming of lignocellulose to H_2 with a CdS/CdO_x photocatalyst, Nat. Energy 2 (2017) 17021.

[21] J. Wang, P. Kumar, H. Zhao, M.G. Kibria, J. Hu, Polymeric carbon nitride-based photocatalysts for photoreforming of biomass derivatives, Green Chem. 23 (19) (2021) 7435–7457.

[22] H. Luo, J. Barrio, N. Sunny, A. Li, L. Steier, N. Shah, I.E.L. Stephens, M.-M. Titirici, Progress and perspectives in photo- and electrochemical-oxidation of biomass for sustainable chemicals and hydrogen production, Adv. Energy Mater. 11 (2021) 2101180.

[23] T. Uekert, C.M. Pichler, T. Schubert, E. Reisner, Solar-driven reforming of solid waste for a sustainable future, Nature Sustain. 4 (2021) 383–391.

[24] P. Cai, H. Fan, S. Cao, J. Qi, S. Zhang, G. Li, Electrochemical conversion of corn stover lignin to biomass-based chemicals between Cu/NiMoCo cathode and Pb/PbO_2 anode in alkali solution, Electrochim. Acta 264 (2018) 128–139.

[25] J. Xu, P. Zhou, C. Zhang, L. Yuan, X. Xiao, L. Dai, K. Huo, Striding the threshold of photocatalytic lignin-first biorefining via a bottom-up approach: from model compounds to realistic lignin, Green Chem. 24 (2022) 5351–5378.

[26] P. Kumar, A. Shayesteh Zeraati, S. Roy, K.A. Miller, A. Wang, L.B. Alemany, T. A. Al-Attas, D. Trivedi, P.M. Ajayan, J. Hu, M.G. Kibria, Metal-free sulfonate/sulfate-functionalized carbon nitride for direct conversion of glucose to levulinic acid, ACS Sustain. Chem. Eng. 10 (19) (2022) 6230–6243.

[27] U. Nwosu, A. Wang, B. Palma, H. Zhao, M.A. Khan, M.d. Kibria, J. Hu, Selective biomass photoreforming for valuable chemicals and fuels: A critical review, Renew. Sustain. Energy Rev. 148 (2021), 111266.

[28] Y.-H. Zhang, S.-Y. Ding, J.R. Mielenz, J.-B. Cui, R.T. Elander, M. Laser, M. E. Himmel, J.R. McMillan, L.R. Lynd, Fractionating recalcitrant lignocellulose at modest reaction conditions, Biotechnol. Bioeng. 97 (2) (2007) 214–223.

[29] M.F. Kuehnel, E. Reisner, Solar hydrogen generation from lignocellulose, Angew. Chem. Int. Ed. 57 (13) (2018) 3290–3296.

[30] T.E. Amidon, S. Liu, Water-based woody biorefinery, Biotechnol. Adv. 27 (5) (2009) 542–550.

[31] J.-P. Lange, Lignocellulose conversion: an introduction to chemistry, process and economics, Biofuels, Bioprod. Biorefin. 1 (1) (2007) 39–48.

[32] C.-H. Zhou, X. Xia, C.-X. Lin, D.-S. Tong, J. Beltramini, Catalytic conversion of lignocellulosic biomass to fine chemicals and fuels, Chem. Soc. Rev. 40 (2011) 5588–5617.

[33] P. Gallezot, Conversion of biomass to selected chemical products, Chem. Soc. Rev. 41 (4) (2012) 1538–1558.

[34] T.DH. Bugg, M. Ahmad, E.M. Hardiman, R. Singh, The emerging role for bacteria in lignin degradation and bio-product formation, Curr. Opin. Biotechnol. 22 (3) (2011) 394–400.

[35] D.W. Cho, R. Parthasarathi, A.S. Pimentel, G.D. Maestas, H.J. Park, U.C. Yoon, D. Dunaway-Mariano, S. Gnanakaran, P. Langan, P.S. Mariano, Nature and kinetic analysis of carbon−carbon bond fragmentation reactions of cation radicals derived from SET-oxidation of lignin model compounds, J. Org. Chem. 75 (19) (2010) 6549–6562.

[36] A.T.W.M. Hendriks, G. Zeeman, Pretreatments to enhance the digestibility of lignocellulosic biomass, Bioresour. Technol. 100 (1) (2009) 10–18.

[37] G.W. Huber, S. Iborra, A. Corma, Synthesis of transportation fuels from biomass: chemistry, catalysts, and engineering, Chem. Rev. 106 (2006) 4044–4098.

[38] S. Zinoviev, F. Müller-Langer, P. Das, N. Bertero, P. Fornasiero, M. Kaltschmitt, G. Centi, S. Miertus, Next-generation biofuels: survey of emerging technologies and sustainability issues, ChemSusChem 3 (2010) 1106–1133.

[39] R. French, S. Czernik, Catalytic pyrolysis of biomass for biofuels production, Fuel Process. Technol. 91 (1) (2010) 25–32.

[40] M.W. Jarvis, J.W. Daily, H.-H. Carstensen, A.M. Dean, S. Sharma, D.C. Dayton, D. J. Robichaud, M.R. Nimlos, Direct detection of products from the pyrolysis of 2-phenethyl phenyl ether, J. Phys. Chem. A 115 (4) (2011) 428–438.

[41] O. Lanzalunga, M. Bietti, Bietti, Photo- and radiation chemical induced degradation of lignin model compounds, J. Photochem. Photobiol. B 56 (2-3) (2000) 85–108.

[42] C.M. Teh, A.R. Mohamed, Roles of titanium dioxide and ion-doped titanium dioxide on photocatalytic degradation of organic pollutants (phenolic compounds and dyes) in aqueous solutions: A review, J. Alloys Compd. 509 (5) (2011) 1648–1660.

[43] S.-H. Li, S. Liu, J.C. Colmenares, Y.-J. Xu, A sustainable approach for lignin valorization by heterogeneous photocatalysis, Green Chem. 18 (3) (2016) 594–607.

[44] P. Lanzafame, G. Centi, S. Perathoner, Catalysis for biomass and CO_2 use through solar energy: Opening new scenarios for a sustainable and low-carbon chemical production, Chem. Soc. Rev. 43 (2014) 7562–7580.

[45] J. Ma, K. Liu, X. Yang, D. Jin, Y. Li, G. Jiao, J. Zhou, R. Sun, Recent advances and challenges in photoreforming of biomass-derived feedstocks into hydrogen, biofuels, or chemicals by using functional carbon nitride photocatalysts, ChemSusChem 14 (22) (2021) 4903–4922.

[46] C.Y. Toe, C. Tsounis, J. Zhang, H. Masood, D. Gunawan, J. Scott, R. Amal, Advancing photoreforming of organics: highlights on photocatalyst and system designs for selective oxidation reactions, Energy Environ. Sci. 14 (2021) 1140–1175.

[47] G. Han, Y.-H. Jin, R.A. Burgess, N.E. Dickenson, X.-M. Cao, Y. Sun, Visible-light-driven valorization of biomass intermediates integrated with H_2 production catalyzed by ultrathin Ni/CdS nanosheets, J. Am. Chem. Soc. 139 (44) (2017) 15584–15587.

[48] Q. Liu, F. Wang, Y. Jiang, W. Chen, R. Zou, J. Ma, L. Zhong, X. Peng, Efficient photoreforming of lignocellulose into H_2 and photocatalytic CO_2 reduction via in-plane surface dyadic heterostructure of porous polymeric carbon nitride, Carbon 170 (2020) 199–212.

[49] J. Gong, A. Imbault, R. Farnood, The promoting role of bismuth for the enhanced photocatalytic oxidation of lignin on Pt-TiO_2 under solar light illumination, Appl. Catal., B 204 (2017) 296–303.

[50] N. Luo, M. Wang, H. Li, J. Zhang, T. Hou, H. Chen, X. Zhang, J. Lu, F. Wang, Visible-light-driven self-hydrogen transfer hydrogenolysis of lignin models and extracts into phenolic products, ACS Catal. 7 (7) (2017) 4571–4580.

[51] J.C. Colmenares, R. Luque, Heterogeneous photocatalytic nanomaterials: Prospects and challenges in selective transformations of biomass-derived compounds, Chem. Soc. Rev. 43 (2014) 765–778.

[52] L.I. Granone, F. Sieland, N. Zheng, R. Dillert, D.W. Bahnemann, Photocatalytic conversion of biomass into valuable products: A meaningful approach? Green Chem. 20 (2018) 1169–1192.

[53] F.H. Isikgor, C.R. Becer, Lignocellulosic biomass: A sustainable platform for the production of bio-based chemicals and polymers, Polym. Chem. 6 (2015) 4497–4559.

[54] W. Schutyser, T. Renders, S. Van den Bosch, S.F. Koelewijn, G.T. Beckham, B. F. Sels, Chemicals from lignin: An interplay of lignocellulose fractionation, depolymerisation, and upgrading, Chem. Soc. Rev. 47 (2018) 852–908.

[55] X.-J. Shen, J.-L. Wen, Q.-Q. Mei, X. Chen, D. Sun, T.-Q. Yuan, R.-C. Sun, Facile fractionation of lignocelluloses by biomass-derived deep eutectic solvent (DES) pretreatment for cellulose enzymatic hydrolysis and lignin valorization, Green Chem. 21 (2) (2019) 275–283.

[56] J.D. Nguyen, B.S. Matsuura, C.R.J. Stephenson, A photochemical strategy for lignin degradation at room temperature, J. Am. Chem. Soc. 136 (4) (2014) 1218–1221.

[57] Y. Nishiyama, P. Langan, H. Chanzy, Crystal structure and hydrogen-bonding system in cellulose Iβ from synchrotron X-ray and neutron fiber diffraction, J. Am. Chem. Soc. 124 (31) (2002) 9074–9082.

[58] X. Liu, X. Duan, W. Wei, S. Wang, B.-J. Ni, Photocatalytic conversion of lignocellulosic biomass to valuable products, Green Chem. 21 (16) (2019) 4266–4289.

[59] S. Bhowmik, S. Darbha, Advances in solid catalysts for selective hydrogenolysis of glycerol to 1,3-propanediol, Catal. Rev. 63 (4) (2021) 639–703.

[60] P. Azadi, O.R. Inderwildi, R. Farnood, D.A. King, Liquid fuels, hydrogen and chemicals from lignin: A critical review, Renew. Sustain. Energy Rev. 21 (2013) 506–523.

[61] F.G. Calvo-Flores, J.A. Dobado, Lignin as renewable raw material, ChemSusChem 3 (11) (2010) 1227–1235.

[62] A.U. Buranov, G. Mazza, Lignin in straw of herbaceous crops, Ind. Crops Prod. 28 (3) (2008) 237–259.

[63] C. Li, X. Zhao, A. Wang, G.W. Huber, T. Zhang, Catalytic transformation of lignin for the production of chemicals and fuels, Chem. Rev. 115 (21) (2015) 11559–11624.

[64] J. Zakzeski, P.C.A. Bruijnincx, A.L. Jongerius, B.M. Weckhuysen, The catalytic valorization of lignin for the production of renewable chemicals, Chem. Rev. 110 (6) (2010) 3552–3599.

[65] I. Bosque, G. Magallanes, M. Rigoulet, M.D. Kärkäs, C.R.J. Stephenson, Redox catalysis facilitates lignin depolymerization, ACS Cent. Sci. 3 (6) (2017) 621–628.

[66] P.J. Deuss, K. Barta, From models to lignin: Transition metal catalysis for selective bond cleavage reactions, Coord. Chem. Rev. 306 (2016) 510–532.

[67] S. Gazi, Valorization of wood biomass-lignin via selective bond scission: A minireview, Appl. Catal., B 257 (2019), 117936.

[68] N. Luo, M. Wang, H. Li, J. Zhang, H. Liu, F. Wang, Photocatalytic oxidation–hydrogenolysis of lignin β-O-4 models via a dual light wavelength switching strategy, ACS Catal. 6 (11) (2016) 7716–7721.

[69] M.V. Galkin, J.S. Samec, Lignin valorization through catalytic lignocellulose fractionation: A fundamental platform for the future biorefinery, ChemSusChem 9 (2016) 1544–1558.

[70] C.S. Lancefield, O.S. Ojo, F. Tran, N.J. Westwood, Isolation of functionalized phenolic monomers through selective oxidation and C-O bond cleavage of the β-O-4 linkages in lignin, Angew. Chem. Int. Ed. Engl. 54 (1) (2015) 258–262.

[71] L.i. Shuai, M.T. Amiri, Y.M. Questell-Santiago, F. Héroguel, Y. Li, H. Kim, R. Meilan, C. Chapple, J. Ralph, J.S. Luterbacher, Formaldehyde stabilization facilitates lignin monomer production during biomass depolymerization, Science 354 (6310) (2016) 329–333.

[72] E. Taarning, C.M. Osmundsen, X. Yang, B. Voss, S.I. Andersen, C.H. Christensen, Zeolite-catalyzed biomass conversion to fuels and chemicals, Energy Environ. Sci. 4 (3) (2011) 793–804.

[73] D. Son, S. Gu, J.-W. Choi, D.J. Suh, J. Jae, J. Choi, J.-M. Ha, Production of phenolic hydrocarbons from organosolv lignin and lignocellulose feedstocks of hardwood, softwood, grass and agricultural waste, J. Ind. Eng. Chem. 69 (2019) 304–314.

[74] C.O. Tuck, E. Pérez, I.T. Horváth, R.A. Sheldon, M. Poliakoff, Valorization of biomass: Deriving more value from waste, Science 337 (2012) 695–699.

[75] N.a. Zhong, R. Chandra, J.N. Saddler, Sulfite post-treatment to simultaneously detoxify and improve the enzymatic hydrolysis and fermentation of a steam-pretreated softwood lodgepole pine whole slurry, ACS Sustain. Chem. Eng. 7 (5) (2019) 5192–5199.

[76] H. Zhao, J. Liu, N. Zhong, S. Larter, Y. Li, M.G. Kibria, B.-L. Su, Z. Chen, J. Hu, Biomass photoreforming for hydrogen and value-added chemicals co-production on hierarchically porous photocatalysts, Adv. Energy Mater. (2023), 2300257.

[77] A.K. Kumar, S. Sharma, Recent updates on different methods of pretreatment of lignocellulosic feedstocks: A review, Bioresour. Bioprocess. 4 (2017) 1–19.

[78] H.K. Sharma, C. Xu, W. Qin, Biological pretreatment of lignocellulosic biomass for biofuels and bioproducts: An overview, Waste Biomass Valori. 10 (2) (2019) 235–251.

[79] X. Wu, H. Zhao, M.A. Khan, P. Maity, T. Al-Attas, S. Larter, Q. Yong, O. F. Mohammed, M.G. Kibria, J. Hu, Sunlight-driven biomass photorefinery for coproduction of sustainable hydrogen and value-added biochemicals, ACS Sustain. Chem. Eng. 8 (41) (2020) 15772–15781.

[80] D. Klemm, B. Heublein, H.-P. Fink, A. Bohn, Cellulose: Fascinating biopolymer and sustainable raw material, Angew. Chem. Int. Ed. 44 (22) (2005) 3358–3393.

[81] Y. Qin, H. Li, J. Lu, F. Meng, C. Ma, Y. Yan, M. Meng, Nitrogen-doped hydrogenated TiO_2 modified with CdS nanorods with enhanced optical absorption, charge separation and photocatalytic hydrogen evolution, Chem. Eng. J. 384 (2020), 123275.

[82] X. Fu, J. Long, X. Wang, D.Y.C. Leung, Z. Ding, L. Wu, Z. Zhang, Z. Li, X. Fu, Photocatalytic reforming of biomass: A systematic study of hydrogen evolution from glucose solution, Int. J. Hydrog. Energy 33 (2008) 6484–6491.

[83] M.R. Hoffmann, S.T. Martin, W. Choi, D.W. Bahnemann, Environmental applications of semiconductor photocatalysis, Chem. Rev. 95 (1) (1995) 69–96.

[84] B. Kraeutler, A.J. Bard, Heterogeneous photocatalytic synthesis of methane from acetic acid - new Kolbe reaction pathway, J. Am. Chem. Soc. 100 (7) (1978) 2239–2240.

[85] P. Gomathisankar, D. Yamamoto, H. Katsumata, T. Suzuki, S. Kaneco, Photocatalytic hydrogen production with aid of simultaneous metal deposition using titanium dioxide from aqueous glucose solution, Int. J. Hydrog. Energy 38 (14) (2013) 5517–5524.

[86] G. Wu, T. Chen, G. Zhou, X. Zong, C. Li, H_2 production with low CO selectivity from photocatalytic reforming of glucose on metal/TiO_2 catalysts, Sci. China Ser. B: Chem. 51 (2008) 97–100.

[87] M.R. St. John, A.J. Furgala, A.F. Sammells, Sammells, Hydrogen generation by photocatalytic oxidation of glucose by platinized n-titania powder, J. Phys. Chem. 87 (5) (1983) 801–805.

[88] A. Caravaca, W. Jones, C. Hardacre, M. Bowker, H_2 production by the photocatalytic reforming of cellulose and raw biomass using Ni, Pd, Pt and Au on titania, Proc. Math. Phys. Eng. Sci. 472 (2016) 20160054.

[89] N. Luo, Z. Jiang, H. Shi, F. Cao, T. Xiao, P. Edwards, Photo-catalytic conversion of oxygenated hydrocarbons to hydrogen over heteroatom-doped TiO_2 catalysts, Int. J. Hydrog. Energy 34 (1) (2009) 125–129.

[90] L. Zhang, J. Shi, M. Liu, D. Jing, L. Guo, Photocatalytic reforming of glucose under visible light over morphology controlled Cu_2O: Efficient charge separation by crystal facet engineering, Chem. Commun. 50 (2014) 192–194.

[91] G. Carraro, C. Maccato, A. Gasparotto, T. Montini, S. Turner, O.I. Lebedev, V. Gombac, G. Adami, G. Van Tendeloo, D. Barreca, P. Fornasiero, Enhanced hydrogen production by photoreforming of renewable oxygenates through nanostructured Fe_2O_3 polymorphs, Adv. Funct. Mater. 24 (3) (2014) 372–378.

[92] Y. Li, J. Wang, S. Peng, G. Lu, S. Li, Photocatalytic hydrogen generation in the presence of glucose over ZnS-coated $ZnIn_2S_4$ under visible light irradiation, Int. J. Hydrog. Energy 35 (13) (2010) 7116–7126.

[93] X. Xu, J. Zhang, S. Wang, Z. Yao, H. Wu, L. Shi, Y. Yin, S. Wang, H. Sun, Photocatalytic reforming of biomass for hydrogen production over ZnS nanoparticles modified carbon nitride nanosheets, J. Colloid Interface Sci. 555 (2019) 22–30.

[94] V.-C. Nguyen, N.-J. Ke, L.D. Nam, B.-S. Nguyen, Y.-K. Xiao, Y.-L. Lee, H. Teng, Photocatalytic reforming of sugar and glucose into H_2 over functionalized graphene dots, J. Mater. Chem. A 7 (14) (2019) 8384–8393.

[95] J.C. Colmenares, A. Magdziarz, A. Bielejewska, High-value chemicals obtained from selective photo-oxidation of glucose in the presence of nanostructured titanium photocatalysts, Bioresour. Technol. 102 (24) (2011) 11254–11257.

[96] B. Zhang, J. Li, L. Guo, Z. Chen, C. Li, Photothermally promoted cleavage of β-1,4-glycosidic bonds of cellulosic biomass on Ir/HY catalyst under mild conditions, Appl. Catal., B 237 (2018) 660–664.

[97] B.C.E. Makhubela, J. Darkwa, The role of noble metal catalysts in conversion of biomass and bio-derived intermediates to fuels and chemicals, Johnson Matthey, Technol. Rev. 62 (1) (2018) 4–31.

[98] L. Wang, Z. Zhang, L. Zhang, S. Xue, W.O.S. Doherty, I.M. O'Hara, X. Ke, Sustainable conversion of cellulosic biomass to chemicals under visible-light irradiation, RSC Adv. 5 (104) (2015) 85242–85247.

[99] A. Speltini, M. Sturini, D. Dondi, E. Annovazzi, F. Maraschi, V. Caratto, A. Profumo, A. Buttafava, Sunlight-promoted photocatalytic hydrogen gas evolution from water-suspended cellulose: A systematic study, Photochem. Photobio. Sci. 13 (10) (2014) 1410–1419.

[100] H. Hao, L. Zhang, W. Wang, S. Zeng, Facile modification of titania with nickel sulfide and sulfate species for the photoreformation of cellulose into hydrogen, ChemSusChem 11 (16) (2018) 2810–2817.

[101] L. Zhang, W. Wang, S. Zeng, Y. Su, H. Hao, Enhanced H_2 evolution from photocatalytic cellulose conversion based on graphitic carbon layers on TiO_2/NiO_x, Green Chem. 20 (13) (2018) 3008–3013.

[102] G. Zhang, C. Ni, X. Huang, A. Welgamage, L.A. Lawton, P.K.J. Robertson, J.T. S. Irvine, Simultaneous cellulose conversion and hydrogen production assisted by cellulose decomposition under UV-light photocatalysis, Chem. Commun. 52 (8) (2016) 1673–1676.

[103] D. Ke, S. Liu, K.e. Dai, J. Zhou, L. Zhang, T. Peng, CdS/regenerated cellulose nanocomposite films for highly efficient photocatalytic H_2 production under visible light irradiation, J. Phys. Chem. C 113 (36) (2009) 16021–16026.

[104] Y. Li, Studies on Cellulose Hydrolysis and Hemicellulose Monosaccharide Degradation in Concentrated Hydrochloric Acid, University of Ottawa, 2014.

[105] A. Zoghlami, G. Paës, Lignocellulosic biomass: Understanding recalcitrance and predicting hydrolysis, Front. Chem. 7 (2019).

[106] V. Dhyani, T. Bhaskar, A comprehensive review on the pyrolysis of lignocellulosic biomass, Renew. Energy 129 (2018) 695–716.

[107] M. Raita, W. Wanmolee, N. Suriyachai, J. Payomhorm, N. Laosiripojana, 3 - Lignocellulosic biomass and its potential derivative products, in: N. Thongchul, A. Kokossis, S. Assabumrungrat (Eds.), A-Z of Biorefinery, (2022) 79-120.

[108] K. Liu, J. Ma, X. Yang, D. Jin, Y. Li, G. Jiao, S. Yao, S. Sun, R. Sun, Boosting electron kinetics of anatase TiO_2 with carbon nanosheet for efficient photo-reforming of xylose into biomass-derived organic acids, J. Alloys Compd. 906 (2022), 164276.

[109] X. Li, Q. Liu, J. Ma, K. Liu, Z. Liu, R. Sun, Entire and efficient utilization of biomass conversion and water splitting via ternary RuP_2/$Ti_4P_6O_{23}$@TiO_2 heterojunction, SSRN 4160383 (2022).

[110] J. Ma, Y. Li, D. Jin, X. Yang, G. Jiao, K. Liu, S. Sun, J. Zhou, R. Sun, Reasonable regulation of carbon/nitride ratio in carbon nitride for efficient photocatalytic reforming of biomass-derived feedstocks to lactic acid, Appl. Catal., B 299 (2021), 120698.

[111] J. Zhang, Z. Xie, Z. Ali, N. Li, Q. Liu, W. Fan, J. Ma, R. Sun, Oxygen-doped carbon nitride nanocages with efficient photon-to-electron conversion for selective oxidation of xylose/xylan to yield xylonic acid, Paper and Biomater. 8 (2023) 53–65.

[112] Z. Liu, K. Liu, R. Sun, J. Ma, Biorefinery-assisted ultra-high hydrogen evolution via metal-free black phosphorus sensitized carbon nitride photocatalysis, Chem. Eng. J. 446 (2022), 137128.

[113] J. Ma, X. Li, Y. Li, G. Jiao, H. Su, D. Xiao, S. Zhai, R. Sun, Single-atom zinc catalyst for co-production of hydrogen and fine chemicals in soluble biomass solution, Adv. Powder Mater. 1 (2022), 100058.

[114] K. Liu, Z. Liu, S. Yao, S. Sun, J. Ma, R. Sun, $CuInS_2$ quantum dots anchored onto the three-dimensional flexible self-supporting graphene oxide array with regulatable crystallinity and defect density for efficient photocatalytic synthesis of xylonic acid, Appl. Catal., B 316 (2022), 121573.

[115] M. Wang, F. Wang, Lignin: catalytic scissoring of lignin into aryl monomers, Adv. Mater. 31 (2019) 1970355.

[116] J. Wang, X. Wang, H. Zhao, J.F. Van Humbeck, B.N. Richtik, M.R. Dolgos, A. Seifitokaldani, M.G. Kibria, J. Hu, Selective C3–C4 cleavage via glucose photoreforming under the effect of nucleophilic dimethyl sulfoxide, ACS Catal. 12 (22) (2022) 14418–14428.

[117] M.-y. Wu, J.-T. Lin, Z.-Q. Xu, T.-c. Hua, Y.-C. Lv, Y.-F. Liu, R.-H. Pei, Q. Wu, M.-H. Liu, Selective catalytic degradation of a lignin model compound into phenol over transition metal sulfates, RSC Adv. 10 (5) (2020) 3013–3019.

[118] B.M. Upton, A.M. Kasko, Strategies for the conversion of lignin to high-value polymeric materials: Review and perspective, Chem. Rev. 116 (4) (2016) 2275–2306.

[119] S. Kim, S.C. Chmely, M.R. Nimlos, Y.J. Bomble, T.D. Foust, R.S. Paton, G. T. Beckham, Computational study of bond dissociation enthalpies for a large range of native and modified lignins, J. Phys. Chem. Lett. 2 (22) (2011) 2846–2852.

[120] J.M. Nichols, L.M. Bishop, R.G. Bergman, J.A. Ellman, Catalytic C−O bond cleavage of 2-aryloxy-1-arylethanols and its application to the depolymerization of lignin-related polymers, J. Am. Chem. Soc. 132 (36) (2010) 12554–12555.

[121] F. Gao, J.D. Webb, H. Sorek, D.E. Wemmer, J.F. Hartwig, Fragmentation of lignin samples with commercial Pd/C under ambient pressure of hydrogen, ACS Catal. 6 (11) (2016) 7385–7392.

[122] M.V. Galkin, J.S.M. Samec, Selective route to 2-propenyl aryls directly from wood by a tandem organosolv and palladium-catalysed transfer hydrogenolysis, ChemSusChem 7 (8) (2014) 2154–2158.

[123] H. Fan, Y. Yang, J. Song, Q. Meng, T. Jiang, G. Yang, B. Han, Free-radical conversion of a lignin model compound catalyzed by Pd/C, Green Chem. 17 (8) (2015) 4452–4458.

[124] M. Wang, J. Lu, X. Zhang, L. Li, H. Li, N. Luo, F. Wang, Two-step, catalytic C-C bond oxidative cleavage process converts lignin models and extracts to aromatic acids, ACS Catal. 6 (9) (2016) 6086–6090.

[125] J. Luo, X. Zhang, J. Lu, J. Zhang, Fine tuning the redox potentials of carbazolic porous organic frameworks for visible-light photoredox catalytic degradation of lignin β-O-4 models, ACS Catal. 7 (8) (2017) 5062–5070.

[126] Y.u. Cao, N. Wang, X. He, H.-R. Li, L.-N. He, Photocatalytic oxidation and subsequent hydrogenolysis of lignin β-O-4 models to aromatics promoted by in situ carbonic acid, ACS Sustain. Chem. Eng. 6 (11) (2018) 15032–15039.

[127] Y. Shiraishi, Y. Togawa, D. Tsukamoto, S. Tanaka, T. Hirai, Highly efficient and selective hydrogenation of nitroaromatics on photoactivated rutile titanium dioxide, ACS Catal. 2 (12) (2012) 2475–2481.

[128] J. Fang, P. Ye, M. Wang, D. Wu, A. Xu, X. Li, Hydrogenolysis and hydrogenation of β-O-4 ketones by a simple photocatalytic hydrogen transfer reaction, Catal. Commun. 107 (2018) 18–23.

[129] J. Dai, A.F. Patti, G.N. Styles, S. Nanayakkara, L. Spiccia, F. Arena, C. Italiano, K. Saito, Lignin oxidation by MnO_2 under the irradiation of blue light, Green Chem. 21 (8) (2019) 2005–2014.

[130] F. Arena, B. Gumina, A.F. Lombardo, C. Espro, A. Patti, L. Spadaro, L. Spiccia, Nanostructured MnO_x catalysts in the liquid phase selective oxidation of benzyl alcohol with oxygen: Part I. Effects of Ce and Fe addition on structure and reactivity, Appl. Catal., B 162 (2015) 260–267.

[131] H. Cao, S.L. Suib, Highly efficient heterogeneous photooxidation of 2-propanol to acetone with amorphous manganese oxide catalysts, J. Am. Chem. Soc. 116 (12) (1994) 5334–5342.

[132] L. Duan, B. Sun, M. Wei, S. Luo, F. Pan, A. Xu, X. Li, Catalytic degradation of acid orange 7 by manganese oxide octahedral molecular sieves with peroxymonosulfate under visible light irradiation, J. Hazard. Mater. 285 (2015) 356–365.

[133] S. Ma, J. Liu, S. Li, B.o. Chen, J. Cheng, J. Kuang, Y.u. Liu, B. Wan, Y. Wang, J. Ye, Q. Yu, W. Yuan, S. Yu, Development of a general and practical iron nitrate/TEMPO-catalyzed aerobic oxidation of alcohols to aldehydes/ketones: catalysis with table salt, Adv. Synth. Catal. 353 (6) (2011) 1005–1017.

[134] S. Son, F.D. Toste, Non-oxidative vanadium-catalyzed C-O bond cleavage: Application to degradation of lignin model compounds, Angew. Chem. Int. Ed. 49 (2010) 3791–3794.

[135] H. Liu, H. Li, J. Lu, S. Zeng, M. Wang, N. Luo, S. Xu, F. Wang, Photocatalytic cleavage of C-C bond in lignin models under visible light on mesoporous graphitic carbon nitride through π–π stacking interaction, ACS Catal. 8 (6) (2018) 4761–4771.

[136] X. Wu, X. Fan, S. Xie, J. Lin, J. Cheng, Q. Zhang, L. Chen, Y. Wang, Solar energy-driven lignin-first approach to full utilization of lignocellulosic biomass under mild conditions, Nat. Catal. 1 (2018) 772–780.

[137] X. Wu, S. Xie, C. Liu, C. Zhou, J. Lin, J. Kang, Q. Zhang, Z. Wang, Y.e. Wang, Ligand-controlled photocatalysis of CdS quantum dots for lignin valorization under visible light, ACS Catal. 9 (9) (2019) 8443–8451.

[138] H. Yoo, M.-W. Lee, S. Lee, J. Lee, S. Cho, H. Lee, H.G. Cha, H.S. Kim, Enhancing photocatalytic β-O-4 bond cleavage in lignin model compounds by silver-exchanged cadmium sulfide, ACS Catal. 10 (15) (2020) 8465–8475.

[139] G. Han, T. Yan, W. Zhang, Y.C. Zhang, D.Y. Lee, Z. Cao, Y. Sun, Highly selective photocatalytic valorization of lignin model compounds using ultrathin metal/CdS, ACS Catal. 9 (12) (2019) 11341–11349.

[140] J. Lin, X. Wu, S. Xie, L. Chen, Q. Zhang, W. Deng, Y.e. Wang, Visible-light-driven cleavage of C−O linkage for lignin valorization to functionalized aromatics, ChemSusChem 12 (22) (2019) 5023–5031.

[141] N. Skillen, H. Daly, L. Lan, M. Aljohani, C.W.J. Murnaghan, X. Fan, C. Hardacre, G.N. Sheldrake, P.K.J. Robertson, Photocatalytic reforming of biomass: What role will the technology play in future energy systems, Top. Curr. Chem. 380 (2022) 33.

[142] C.W. Murnaghan, N. Skillen, C. Hardacre, J. Bruce, G.N. Sheldrake, P. K. Robertson, Exploring lignin valorisation: The application of photocatalysis for the degradation of the β-5 linkage, J. Phys. Energy 3 (2021), 035002.

[143] K. Shimura, H. Yoshida, Heterogeneous photocatalytic hydrogen production from water and biomass derivatives, Energy Environ. Sci. 4 (2011) 2467–2481.

[144] Y. Xu, M.A.A. Schoonen, The absolute energy positions of conduction and valence bands of selected semiconducting minerals, Am. Mineral. 85 (3-4) (2000) 543–556.

[145] R. Williams, M.E. Labib, Zinc sulfide surface chemistry: an electrokinetic study, J. Colloid Interface Sci. 106 (1) (1985) 251–254.

[146] S.R. Kadam, V.R. Mate, R.P. Panmand, L.K. Nikam, M.V. Kulkarni, R.S. Sonawane, B.B. Kale, A green process for efficient lignin (biomass) degradation and hydrogen production via water splitting using nanostructured C, N, S-doped ZnO under solar light, RSC Adv. 4 (105) (2014) 60626–60635.

[147] C. Li, H. Wang, S.B. Naghadeh, J.Z. Zhang, P. Fang, Visible light driven hydrogen evolution by photocatalytic reforming of lignin and lactic acid using one-dimensional NiS/CdS nanostructures, Appl. Catal., B 227 (2018) 229–239.

[148] K. Kobayakawa, Y. Sato, S. Nakamura, A. Fujishima, Photodecomposition of kraft lignin catalyzed by titanium dioxide, Bull. Chem. Soc. Jpn. 62 (11) (1989) 3433–3436.

[149] H. Kasap, D.S. Achilleos, A. Huang, E. Reisner, Photoreforming of lignocellulose into H_2 using nanoengineered carbon nitride under benign conditions, J. Am. Chem. Soc. 140 (37) (2018) 11604–11607.